

THE SUPERNOVA DELAY TIME DISTRIBUTION IN GALAXY CLUSTERS AND IMPLICATIONS FOR TYPE-IA PROGENITORS AND METAL ENRICHMENT^{*}

DAN MAOZ¹, KEREN SHARON², AVISHAY GAL-YAM³

Draft version August 25, 2010

ABSTRACT

Knowledge of the supernova (SN) delay time distribution (DTD) – the SN rate versus time that would follow a hypothetical brief burst of star formation – can shed light on SN progenitors and physics, as well as on the timescales of chemical enrichment in different environments. We compile recent measurements of the Type-Ia SN (SN Ia) rate in galaxy clusters at redshifts from $z = 0$ out to $z = 1.45$, just 2 Gyr after cluster star formation at $z \approx 3$. We review the plausible range for the observed total iron-to-stellar mass ratio in clusters, based on the latest data and analyses, and use it to constrain the time-integrated number of SN Ia events in clusters. With these data, we recover the DTD of SNe Ia in cluster environments. The DTD is sharply peaked at the shortest time-delay interval we probe, $0 < t < 2.2$ Gyr, with a low tail out to delays of ~ 10 Gyr, and is remarkably consistent with several recent DTD reconstructions based on different methods, applied to different environments. We test DTD models from the literature, requiring that they simultaneously reproduce the observed cluster SN rates and the observed iron-to-stellar mass ratios. A parametrized power-law DTD of the form $t^{-1.2 \pm 0.3}$ from $t = 400$ Myr to a Hubble time, can satisfy both constraints. Shallower power laws, such as $t^{-1/2}$ cannot, assuming a single DTD, and a single star-formation burst (either brief or extended) at high z . This implies 50–85% of SNe Ia explode within 1 Gyr of star formation. DTDs from double-degenerate (DD) models, which generically have $\sim t^{-1}$ shapes over a wide range of timescales, match the data, but only if their predictions are scaled up by factors of 5 – 10. Single degenerate (SD) DTDs always give poor fits to the data, due to a lack of delayed SNe and overall low numbers of SNe. The observations can also be reproduced with a combination of two SN Ia populations – a prompt SD population of SNe Ia that explodes within a few Gyr of star formation, and produces about 60 percent of the iron mass in clusters, and a DD population that contributes the events seen at $z < 1.5$. An alternative scenario of a single, prompt, SN Ia population, but a composite star-formation history in clusters, consisting of a burst at high z , followed by a constant star-formation rate, can reproduce the SN rates, but is at odds with direct measurements of star formation in clusters at $0 < z < 1$. Our results support the existence of a DD progenitor channel for SNe Ia, if the overall predicted numbers can be suitably increased.

Subject headings: supernovae: general – galaxies: clusters: general

1. INTRODUCTION

Supernovae (SNe) play a central role in astrophysics, not only as distance indicators for cosmology (e.g., Riess et al. 1998; Perlmutter et al. 1999), but as prime synthesizers of heavy elements (e.g. Woosley 2007), sources of kinetic energy, and accelerators of cosmic rays (e.g. Helder et al. 2009). However, many of the most basic facts about these events are still poorly understood. Core-collapse (CC) SNe are descended from massive stars, roughly in the range $8 - 50 M_{\odot}$ (e.g. Gal-Yam & Leonard 2009), but the exact limits are not known, neither from theory nor from observation. It is not yet clear what are the physical parameters (mass, binarity, rotation, magnetic field, and more) that determine the

variety of observed CC-SN subtypes (IIP, Ib, Ic, IIn, IIL; see Filippenko 1997, for a review). Type-Ia SNe (SNe Ia) are linked by indirect evidence to the thermonuclear detonations of carbon-oxygen white dwarfs (WDs) whose mass has grown to near the Chandrasekhar limit (Hoyle & Fowler 1960). However, competing scenarios exist for the initial conditions and evolutionary paths that lead to this mass growth. In the single degenerate (SD) model (Whelan & Iben 1974) a WD grows in mass through accretion from a non-degenerate stellar companion. In the double degenerate (DD) model (Iben & Tutukov 1984; Webbink 1984), two WDs merge after losing energy and angular momentum to gravitational waves. In both scenarios, many questions remain regarding the ignition and development of the explosion itself. It is only recently that the relative and absolute rates of CC SNe and SNe Ia as a function of environment and cosmic time are starting to be measured accurately, and therefore the respective quantity, types, and times of their contributions to metal enrichment history are still poorly constrained.

A fundamental function that could shed light on all of these issues is the SN delay time distribution (DTD). The DTD is the hypothetical SN rate versus time that would follow a brief burst of star formation. The DTD is directly linked to the lifetimes (i.e., the initial masses) of

^{*} Based on observations made with the NASA/ESA *Hubble Space Telescope*, obtained at the Space Telescope Science Institute, which is operated by the Association of Universities for Research in Astronomy, Inc., under NASA contract NAS 5-26555. These observations are associated with programs GO-10493 and GO-10793.

¹ School of Physics and Astronomy, Tel Aviv University, Tel Aviv 69978, Israel.

² Kavli Institute for Cosmological Physics, The University of Chicago, Chicago, IL 60637.

³ Ben-Ziyo Center for Astrophysics, Faculty of Physics, Weizmann Institute of Science, Rehovot 76100, Israel.

the progenitors and to the binary evolution timescales up to the explosion, and therefore different progenitor scenarios predict different DTDs. Furthermore, the DTDs of different SN types dictate directly the mix of contributions of different SN types to metal enrichment throughout cosmic history. Until recently, only few, and often-contradictory, observational constraints on the DTD existed. One observational approach has been to compare the SN rate in field galaxies, as a function of redshift, to the cosmic star formation history (SFH). Given that the DTD is the SN “response” to a short burst of star formation, the SN rate versus cosmic time will be the convolution of the full SFH with the DTD. Gal-Yam & Maoz (2004) carried out the first such comparison, using a small sample of SNe Ia out to $z = 0.8$, and concluded that the results were strongly dependent on the poorly known cosmic SFH, a conclusion echoed by Forster et al. (2006).

With the availability of SN rate measurements to higher redshifts, Barris & Tonry (2006) found a SN Ia rate that closely tracks the SFH out to $z \sim 1$, and concluded that the DTD must be concentrated at short delays, $\lesssim 1$ Gyr. Similar conclusions have been reached, at least out to $z \sim 0.7$, by Sullivan et al. (2006). In contrast, Dahlen et al. (2004, 2008) and Strolger (2004) have argued for a DTD that is peaked at a delay of ~ 3 Gyr, with little power at short delays, based on a decrease in the SN Ia rate at $z > 1$. However, Kuznetsova et al. (2007) have re-analyzed some of these datasets and concluded that the small numbers of SNe and their potential classification errors preclude reaching a conclusion. Similarly, Poznanski et al. (2007) performed new measurements of the $z > 1$ SN Ia rate, and found that, within uncertainties, the SN rate could be tracking the SFH. This, again, would imply a short delay time. Greggio et al. (2008) pointed out that underestimated extinction of the highest- z SNe, observed in their rest-frame ultraviolet emission, could be an additional factor affecting these results.

A second approach to recovering the DTD has been to compare the SN rates in galaxy populations of different characteristic ages. Using this approach, Mannucci et al. (2005, 2006), Scannapieco & Bildsten (2005), and Sullivan (2006) all found evidence for the co-existence of two SN Ia populations, a “prompt” population that explodes within $\sim 100 - 500$ Myr, and a delayed channel that produces SNe Ia on timescales of order 5 Gyr. Naturally, these two “channels” may in reality be just integrals over a continuous DTD on two sides of some time border (Greggio et al. 2008). Totani et al. (2008) have used a similar approach to recover the DTD, by comparing SN Ia rates in early-type galaxies of different characteristic ages, seen at $z = 0.4 - 1.2$ as part of the Subaru/XMM-Newton Deep Survey (SXDS) project. They find a DTD consistent with a t^{-1} form, which is roughly generic for DD models (e.g. Greggio 2005; see §5.1, below). Additional recent attempts to address the issue with the “rate vs. age” approach have been made by Aubourg et al. (2008), Raskin et al. (2009), Yasuda & Fukugita (2009), and Cooper et al. (2009).

Both of the above approaches involve averaging, and hence some loss of information. In the first approach, one averages over large galaxy populations, by associating all of the SNe detected at a given redshift with

all the galaxies of a particular type at that redshift. In the second approach, a characteristic age for a sample of galaxies replaces the detailed SFH of the individual galaxies in a SN survey. Maoz et al. (2010) recently presented a method for recovering the DTD, which avoids this averaging. In the method, the SFH of every individual galaxy, or even galaxy subunit, is compared to the number of SNe it hosted in the survey (generally none, sometimes one, rarely more). DTD recovery is treated as a linearized inverse problem, which is solved statistically. Maoz et al. (2010) applied the method to a subsample of the galaxies in the Lick Observatory SN Search (Filippenko et al. 2010; Leaman et al. 2010; Li et al. 2010a,b), having SFH reconstructions by Tojeiro et al. (2009) based on data from the Sloan Digital Sky Survey (SDSS; York et al. 2000). Maoz et al. (2010) find a significant detection of both a prompt SN Ia component, that explodes within 420 Myr of star formation, and a delayed SN Ia with population that explodes after > 2.4 Gyr. Maoz & Badenes (2010) applied this method also to a sample of SN remnants in the Magellanic Clouds, compiled by Badenes, Maoz, & Draine (2010). Treating the remnants as an effective SN survey conducted over ~ 20 kyr, they also find a significant detection of a prompt (this time < 330 Myr) SN Ia component. A related DTD reconstruction method has been applied by Brandt et al. (2010) to the SNe Ia from the SDSS II survey. Like Maoz et al. (2010), they detect both a prompt and a delayed SN Ia population.

Yet another approach for recovering the DTD, which is at the focus of this paper, is to measure the SN rate vs. redshift in massive galaxy clusters. The deep potential wells of clusters, combined with their relatively simple SFHs, make them ideal locations for studying both the DTD and the metal production of SNe. Optical spectroscopy and multiwavelength photometry of cluster galaxies has shown consistently that the bulk of their stars were formed within short episodes (~ 100 Myr) at $z \sim 3$ (e.g., Daddi et al. 2000; Stanford et al. 2005; Eisenhardt et al. 2008). Thus, the observed SN rate vs. the elapsed cosmic time since the stellar formation epoch provides an almost (see §5) direct measurement of the form of the DTD. Furthermore, the record of metals stored in the intracluster medium (ICM) constrains the number of SNe that have exploded, and hence the normalization of the DTD.

Renzini et al. (1993) and Renzini (1997) first pointed out that the large mass of iron in the ICM could not have been produced solely by CC SNe from a stellar population with a standard initial mass function (IMF). Either a “top-heavy” IMF, or a dominant contribution by SNe Ia is required. Maoz & Gal-Yam (2004) revisited the problem, and tested the hypothesis that the main source of iron is SNe Ia. Accounting for the CC SN contribution to the observed iron mass, they calculated the number of SNe Ia, per present-day stellar luminosity, needed to have exploded over the entire past history of a cluster, in order to produce the observed iron mass. Finally, they compared some simple theoretical DTDs, normalized to produce this number of SNe, to the then-available cluster SN Ia rates (Gal-Yam, Maoz, & Sharon 2002; Reiss 2000). The low observed SN Ia rates out to $z \sim 1$ implied that the large number of events, needed to produce the bulk of the iron, occurred at even higher redshifts, be-

yond the range of the then-existing observations. Maoz & Gal-Yam (2004) therefore concluded that SNe Ia can be the main source of iron only if most of them explode during the relatively brief time interval between star formation in massive clusters (at $z \sim 2-3$) and the highest-redshift cluster SN rate measurements (at $z \sim 1$). In other words, the majority of SNe Ia (at least those that occur in a galaxy cluster environment) must have a short time delay, $\lesssim 2$ Gyr.

A shortcoming of the work by Maoz & Gal-Yam (2004) was the paucity and quality of the cluster SN rate data it was based on. The low- z cluster SN rate by Reiss (2000) was never published in the refereed literature. The cluster SN rates at $z = 0.25 - 0.9$ by Gal-Yam et al. (2002), were based on very few events – two or three – discovered in archival *Hubble Space Telescope* (HST) WFPC2 images of clusters. The large Poisson and systematic uncertainties in the resulting rates precluded any detailed discrimination among model DTDs.

Over the past few years, the observational situation has improved dramatically. Accurate cluster SN Ia rates have been measured in the redshift range of 0 to 1.5, with smaller errors than the previous sole published study at $\langle z \rangle = 0.25, 0.90$ by Gal-Yam et al. (2002). In this paper, we utilize this wealth of new measurements for a renewed analysis of the cluster SN rate and its implications for the SN Ia DTD and for cluster metal-enrichment history. We show that the new data permit a direct comparison of the observations with the functional behavior of various DTDs that have been proposed in the literature, whether parametrized-mathematical or phenomenological DTDs, or DTDs resulting from physical considerations at different levels of sophistication. We find that few of these models, in their simplest forms, are compatible with the emerging observational picture, and therefore we have reached the point where the observations discriminate among models. In §2, below, we compile the existing cluster SN Ia measurements. In §3, we review the existing measurements of the properties of clusters, particularly the gas-to-stellar mass ratio, that are relevant for estimating the present-day cluster iron-to-stellar mass ratio. This ratio, in turn, sets the number of SN Ia that have exploded in clusters, per unit stellar mass formed, which then fixes the normalization of the DTD. In §4 we use the rates and the normalization to recover the observational DTD. We take a forward-modeling approach starting in §5, where we compare the observed rates to the DTD predictions of various “single-component” models that invoke a single mathematical form or physical progenitor formation channel. In §6, we relax the assumption of a single, instantaneous, star-formation episode in clusters, and examine whether an extended star-formation history, combined with some single DTD, can reproduce the measurements. In §7, we examine the ability of composite models, which mix diverse DTDs, or multiple episodes of star formation, to match the observations. We summarize our results in §8. Throughout the paper we assume a cosmology with parameters $\Omega_\Lambda = 0.7$, $\Omega_m = 0.3$, and $H_0 = 70 \text{ km s}^{-1} \text{ Mpc}^{-1}$.

2. CLUSTER SN IA RATES

2.1. Existing cluster SN rates

To perform our analysis, we first compile the cluster SN Ia rate measurements currently in existence. The recent measurements are at mean redshifts of $\langle z \rangle = 0.02$ (Mannucci et al 2008); $\langle z \rangle = 0.15$ (Sharon et al. 2007; Gal-Yam et al. 2008); $\langle z \rangle = 0.08, 0.23$ (Dilday et al. 2010); $\langle z \rangle = 0.46$ (Graham et al. 2008); $\langle z \rangle = 0.60$ (Sharon et al. 2010); and $\langle z \rangle = 1.12$ (Barbary et al. 2010). The mean redshifts are visibility-time-weighted means for the clusters monitored by each survey, i.e., in the calculation of the mean, the redshift of each cluster in the survey sample is weighted by the effective time during which a SN Ia would have been visible in the survey (see, e.g., Sharon et al. 2007). Before these recent measurements, the sole modern published cluster rates were at $\langle z \rangle = 0.25, 0.90$ (Gal-Yam et al. 2002). Table 1 summarizes, for each of these measurements, the mean redshift of the sample, the redshift range, the cosmic times corresponding to these redshifts in our assumed cosmology, and the SN Ia rate, normalized by stellar mass. The stellar masses, at the cosmic time corresponding to the redshifts of the clusters, have generally been estimated consistently in the respective papers, based on the observed stellar luminosities and colors of the monitored cluster galaxies, and assuming the same IMF – the “diet Salpeter” IMF of Bell et al. (2003). Exceptions to this are: Dilday et al. (2010), who converted their luminosity-normalized rates to mass-normalized rates assuming that the mean M/L_B ratio found by Sharon et al. (2007) is valid for their cluster sample, which spans a similar redshift range; Gal-Yam et al. (2002), whose rates were mass normalized by Sharon et al. (2010), using M/L_B from Sharon et al. (2007) at low z and M/L_B from Sharon et al. (2010) at high z ; and Graham et al. (2008), who estimate masses for the galaxies in their sample using the spectral population synthesis of Buzzoni (2005) who, in turn, assumed a Salpeter (1955) IMF. We therefore scale up the Graham et al. (2008) rate by a factor of 1.77, which is the ratio between the remaining stellar mass in an old and inactive quiescent population in a Salpeter (1955) IMF, and that in a diet-Salpeter IMF (see §3.4, below, for details). We follow Barbary et al. (2010) in scaling up the rate of Sharon et al. (2010) by 35%, to account for the offset in the M/L_g vs. $g-r$ relation of Bell et al. (2003), expected in the younger galaxies that exist at $\langle z \rangle = 0.6$.

2.2. Observed cluster SN Ia rates vs. redshift

Figure 1 shows the rates we have compiled, and which we analyze in this paper. It suggests only a mild rise in the rates, by a factor of $\sim 2-5$, over the redshift interval probed. Remarkably, the cluster SN rate appears not to change much from $z = 0$ to $z = 1.45$, corresponding to a lookback time of 9.8 Gyr. This is only about 2 Gyr after the formation of the cluster stars, assuming this occurred at a redshift $z_f \approx 3$.

3. TIME-INTEGRATED SN NUMBER PER FORMED MASS

As pointed out by Maoz & Gal-Yam (2004) and Sharon et al. (2010), and now further suggested by the results above, the integral over the SN Ia rate from $z = 0$ to $z = 1.45$, times the mean iron yield of SNe Ia ($0.6-0.7M_\odot$; see below), gives just a small fraction, roughly 10%, of the present-day ratio of iron mass to stellar mass observed in clusters. It is then unavoidable that the large majority

TABLE 1
CLUSTER SN Ia RATES AND DELAY TIME DISTRIBUTION

Redshift z (1)	Cosmic time t [Gyr] (2)	SN Ia rate $R_{Ia}(t)$ [SNuM] (3)	Delay τ [Gyr] (4)	DTD $\Psi(\tau)$ (5)	Ref. (6)
$0.020^{+0.020}_{-0.015}$	$13.2^{+0.2}_{-0.3}$	$0.066^{+0.027}_{-0.020}$	$11.1^{+0.2}_{-0.3}$	$3.6^{+1.5}_{-1.1}$	M08
$0.084^{+0.086}_{-0.054}$	$12.4^{+0.6}_{-1.0}$	$0.060^{+0.029}_{-0.021}$	$10.3^{+0.6}_{-1.0}$	$3.3^{+1.6}_{-1.2}$	D10
$0.150^{+0.040}_{-0.090}$	$11.6^{+1.0}_{-0.4}$	$0.098^{+0.068}_{-0.048}$	$9.5^{+1.0}_{-0.4}$	$5.5^{+3.8}_{-2.7}$	S07
$0.225^{+0.075}_{-0.125}$	$10.8^{+1.3}_{-0.7}$	$0.088^{+0.025}_{-0.020}$	$8.7^{+1.3}_{-0.7}$	$4.9^{+1.4}_{-1.1}$	D10
$0.250^{+0.120}_{-0.070}$	$10.5^{+0.7}_{-1.1}$	$0.110^{+0.160}_{-0.070}$	$8.4^{+0.7}_{-1.1}$	$6.2^{+9.0}_{-4.0}$	GY02
$0.460^{+0.140}_{-0.260}$	$8.7^{+2.3}_{-1.0}$	$0.177^{+0.212}_{-0.124}$	$6.6^{+2.3}_{-1.0}$	$10.1^{+12.1}_{-7.1}$	G08
$0.600^{+0.290}_{-0.100}$	$7.8^{+0.7}_{-1.5}$	$0.151^{+0.138}_{-0.116}$	$5.7^{+0.7}_{-1.5}$	$8.7^{+7.9}_{-6.6}$	S10
$0.900^{+0.370}_{-0.070}$	$6.2^{+0.3}_{-1.4}$	$0.220^{+0.250}_{-0.110}$	$4.1^{+0.3}_{-1.4}$	$12.9^{+14.6}_{-19.9}$	GY02
$1.120^{+0.330}_{-0.220}$	$5.3^{+0.9}_{-1.0}$	$0.364^{+0.301}_{-0.270}$	$3.2^{+0.9}_{-1.0}$	$21.6^{+16.0}_{-11.2}$	B10
...	$1.1^{+1.1}_{-1.1}$	230^{+112}_{-112}	txt

(1) – Visibility-time-weighted mean redshift of cluster sample, and redshift range.
(2) – Time since Big Bang corresponding to redshifts in (1).
(3) – SN rate per unit stellar mass, in SNuM (10^{-12} SNe yr $^{-1}$ M $_{\odot}^{-1}$), with normalization relative to remaining mass at the redshift of the observation.
(4) – Time since $z_f = 3$ corresponding to redshifts in (1).
(5) – Mean recovered DTD value in time bin of (4), in units of 10^{-14} SNe yr $^{-1}$ M $_{\odot}^{-1}$, with normalization relative to formed mass.
(6) – References: M08 – Mannucci et al. (2008); D10 – Dilday et al. (2010); S07 – Sharon et al. (2007); GY02 – Gal-Yam et al. (2002); G08 – Graham et al. (2008); S10 – Sharon et al. (2010); B10 – Barbary et al. (2010); txt – DTD value derived in this work, based on iron-mass constraints.
Published rates have been converted to the same “diet Salpeter” IMF (Bell et al. 2003). S10 rate has been scaled up to account for expected evolution of the Bell et al. (2003) M/L -to-color relations, according to B10.

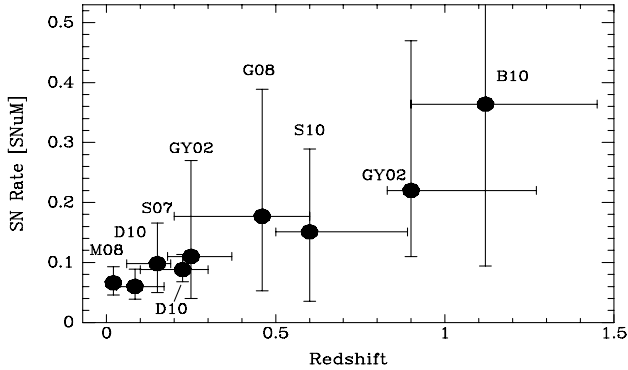


FIG. 1.— SN Ia rates per unit stellar mass in galaxy clusters, as a function of redshift, as listed in Table 1. Observed rates, here and in the subsequent Figs. 3–13, are in units of SNuM: 10^{-12} SNe yr $^{-1}$ M $_{\odot}^{-1}$. Horizontal error bars mark the cluster redshift intervals of the respective SN surveys, with the central value at the visibility-time-weighted mean redshift of each survey. Vertical error bars show the summed 68% confidence limit statistical and systematic uncertainties. All measurements have been consistently scaled to the “diet Salpeter” IMF (see text). Labels are: M08 – Mannucci et al. (2008); D10 – Dilday et al. (2010); S07 – Sharon et al. (2007); GY02 – Gal-Yam et al. (2002); G08 – Graham et al. (2008); S10 – Sharon et al. (2010); B10 – Barbary et al. (2010).

of cluster metals were produced within the first 1-2 Gyrs after the formation of the cluster stars. The metals were produced by CC SNe and perhaps by “prompt” SNe Ia,

but they were not produced by any SNe with a larger delay, as the rate measurements show that only few such explosions took place at those later times.

In order to juxtapose the new cluster rates, compiled above, with model expectations, we revisit the question of the iron-to-stellar mass ratio in clusters, which dictates the normalization of the DTD. In addition to considering the latest data on cluster properties, our treatment will differ from the one in Maoz & Gal-Yam (2004) in several respects, most notably in that we will use mass-normalized, rather than luminosity-normalized SN rates, and we will account for mass evolution due to stellar mass loss. Stellar mass is, of course, more closely related to the number of stars than is blue luminosity, and is a more stable quantity.

The mass of iron in clusters that is attributable to SNe Ia is the sum of the iron masses in the ICM and in stars, minus the mass of iron produced by CC SNe. Thus, the ratio between SN Ia-produced iron mass and the present-day stellar mass is

$$\frac{M_{\text{Fe,Ia}}}{M_{*,0}} = 0.0074 \left[\frac{Z_{\text{Fe},\odot}}{0.0026} \left(\frac{M_{\text{gas}}/M_{*,0}}{10} \frac{Z_{\text{Fe,gas}}}{0.3} + \frac{Z_{\text{Fe},*}}{1.2} \right) - \frac{M(> 8M_{\odot})/M_{*,0}}{0.35} \frac{y_{\text{cc}}}{0.01} \right]. \quad (1)$$

We discuss below each of the quantities that enter this equation.

3.1. The solar iron abundance

The value of the photospheric solar abundance of iron, $Z_{\text{Fe},\odot} = 0.0026$, is from Anders and Grevesse (1989). Although the correct photospheric iron abundance has been revised down to 0.00176 (Grevesse & Sauval 1999), the ICM and stellar abundances we quote below, and which are still generally used in the literature, relate to the Anders and Grevesse (1989) value⁵.

3.2. The gas-to-star mass ratio

The present-day mass ratio of baryons in the ICM gas and in stars, $M_{\text{gas}}/M_{*,0}$, has been recently re-evaluated by Gonzalez, Zaritsky, & Zabludoff (2007), taking into account the contribution to $M_{*,0}$ by the intergalactic stellar population of a cluster. Contrary to Lin et al. (2003), who argued for $M_{\text{gas}}/M_{*,0}$ that is independent of total cluster mass, Gonzalez et al. (2007) find that $M_{\text{gas}}/M_{*,0}$ rises monotonically with cluster mass, from a value of about 5 for low-mass clusters to about 15 for the most-massive systems. To find the suitable values for the clusters from which were derived the SN rates that we analyze, we now examine the typical masses of those clusters.

The most massive cluster sample in our SN rate compilation is that of Sharon et al. (2010), which is largely coincident with the $z > 0.5$ MACS cluster sample of Ebeling et al. (2007). The clusters in this sample have total masses $M_{500} \sim 10^{15} M_{\odot}$, where M_{500} is the mass within a spherical volume in which the mean density is 500 times the critical closure density. In the Sharon et al. (2010) sample, the part of the rest-frame B -band luminosity of each cluster that is included in the HST field of view (and which is therefore monitored for SNe) is $(1-6) \times 10^{12} L_{B,\odot}$, and the corresponding stellar mass range is $(4-17) \times 10^{12} M_{\odot}$, with a mean of $10^{13} M_{\odot}$. Such masses also apply to the massive, X-ray-selected clusters at $\langle z \rangle = 0.25, 0.90$ studied by Gal-Yam et al. (2002). For the $\langle z \rangle = 0.15$ clusters monitored by Gal-Yam et al. (2008), the typical stellar mass is $7 \times 10^{12} M_{\odot}$ (Sharon et al. 2007). From Gonzalez et al. (2007), this corresponds to total masses of $M_{500} \sim 4 \times 10^{14} M_{\odot}$.

Barbary et al. (2010) find, for their $\langle z \rangle = 1.12$ clusters, a mean B -band luminosity, of $\approx 3 \times 10^{12} L_{B,\odot}$, and typical stellar masses of $\approx 4 \times 10^{12} M_{\odot}$. As a check, the bulk properties of the Barbary et al. (2010) clusters, such as X-ray luminosities, X-ray temperatures, and velocity dispersions, also suggest masses about one-half as large as those of the cluster sample of Sharon et al. (2010) at $\langle z \rangle = 0.60$. Well-measured X-ray temperatures exist in the literature for five of the Barbary et al. sample clusters, and are all around 6-7 keV (Rosati et al. 2004; Stanford et al. 2002, 2006; Boehringer et al. 2008; Gilbank et al. 2008). This compares to the mean temperature, $\langle kT \rangle = 9$ keV, of the $z > 0.5$ MACS cluster sample of Ebeling et al. (2007). X-ray luminosities, reported for these five Barbary et al. clusters, and for an additional four of their clusters (Rosati et al. 1999; Postman et al. 2001; Bremer et al. 2006; Andreon et al. 2008) are in the range $\sim 0.7 - 16 \times 10^{44}$ erg s⁻¹, with a mean of \sim

4×10^{44} erg s⁻¹, compared to $\langle L_X \rangle = 16 \times 10^{44}$ erg s⁻¹ for the Ebeling et al. (2007) sample. Galaxy velocity dispersion best-fit measurements for seven of the Barbary et al. clusters are in the range of $\approx 600 - 1300$ km s⁻¹ (references above, plus Eisenhardt et al. 2008; Cain et al. 2008), with a mean of about 850 km s⁻¹, compared to $\langle \sigma \rangle = 1300$ km s⁻¹ for the $z > 0.5$ MACS clusters. Since total mass depends (e.g., Hicks et al. 2008) on X-ray temperature roughly as $M \propto T^{1.5}$, on X-ray luminosity roughly as $M \propto L_X^{0.5}$, and on velocity dispersion as $M \propto \sigma^2$, all of these observables suggest that the typical cluster in the Barbary et al. sample has about one-half the mass of the typical cluster in the Sharon et al. (2010) sample. Assuming a constant fraction of the cluster mass in stars, the stellar mass in the Barbary et al. sample would also be of order one-half that in the Sharon et al. (2010) sample. However, the stellar mass fraction in clusters depends on total cluster mass. For example, Andreon (2010) has recently found a dependence of roughly $f_{\text{stars}} \propto M^{-0.5}$. If this relation held also for clusters at redshifts $z > 1$, the stellar mass in the Barbary et al. clusters would be only about 1.4 times lower than in the Sharon et al. (2010) sample, and thus more similar to the $\langle z \rangle = 0.15$ clusters monitored by Gal-Yam et al. (2008).

The optically selected clusters monitored for SNe by Graham et al. (2008) and Dilday et al. (2010) have masses comparable to those of the samples discussed above, though somewhat lower. Graham et al. (2008) derived a total stellar mass of $M_* = 8 \times 10^{13} M_{\odot}$ for the 30 clusters they used for their SN rate measurement, or $\sim 3 \times 10^{12} M_{\odot}$ for a typical cluster. Dilday et al. (2010) report a total r -band luminosity of $L_r = 10^{14} L_{r,\odot}$ for the 71 clusters in their low- z , “C4”, cluster subsample. Taking $M_*/L_r = 3$ (Sharon et al. 2007), this gives a mean stellar mass per cluster of $\sim 4 \times 10^{12} M_{\odot}$. For the 492 clusters in the $\langle z \rangle = 0.225$ “maxBCG” sample of Dilday et al. (2010), the integrated luminosity is $L_r = 2 \times 10^{14} L_{r,\odot}$, and hence the mean stellar mass per cluster is $\sim 1 \times 10^{12} M_{\odot}$. Thus, this one subsample of Dilday et al. (2010) has clusters that are undermassive, compared to the other cluster samples we analyze. The other samples have only about a factor-3 difference in mean cluster mass between the higher- and lower-mass extremes.

From the fits by Gonzalez et al. (2007), the lower and higher typical masses considered above (excluding the lower-mass maxBCG sample of Dilday et al. 2010) correspond to $M_{\text{gas}}/M_{*,0}$ values of 6.5 and 14.5, respectively. However, Gonzalez et al. (2007) used the relation obtained by Cappellari et al. (2006) between the kinematically measured total-mass-to-luminosity ratio, M/L of nearby ellipticals and their I -band luminosity. Cappellari et al., when comparing their results to M/L estimates for the same galaxies based on spectral population synthesis, concluded that 30% of the contribution to their kinematic M/L could be due to dark matter within the central regions. If so, the stellar masses in clusters found by Gonzalez et al. (2007) would be scaled down by 0.7, and hence $M_{\text{gas}}/M_{*,0}$ would increase to 9.3 for, e.g., the $\langle z \rangle = 0.15$ cluster sample, and to 21 for the $\langle z \rangle = 0.60$ cluster sample.

Laganá et al. (2008) re-analyzed X-ray and optical

⁵ Lin et al. (2003) derived an iron-to-stellar mass ratio, using a fairly low ICM iron abundance of 0.21 solar found by De Grandi & Molendi (2001), but coupled it to the *meteoritic* iron abundance of Anders and Grevesse (1989), 0.00181. As a result, the ratio they found is a factor of ~ 2 lower than we find here.

data for five clusters to deduce the stellar and gas mass fractions. To obtain stellar masses, they used the Kauffmann et al. (2003) M/L ratios, which are consistent with the Bell et al. (2003) M/L ratios, used in deriving the SN rates analyzed here. For clusters with total masses, M_{500} , similar to the two ends of the typical mass range considered here, Laganá et al. (2008) find $M_{\text{gas}}/M_{*,0}$ of about 8 and 17, respectively. Giodini et al. (2009) also recently examined the dependence of stellar and gas mass fractions on M_{500} . Gas mass fractions were estimated for 41 clusters compiled by Pratt et al. (2009) from the literature. Stellar mass fractions were obtained for a sample of 91 groups and poor clusters from the COSMOS survey, based on spectral population synthesis fitting of their spectral energy distributions. These were combined with the re-evaluated stellar masses of 27 clusters from Lin et al. (2003). We scale down their stellar masses by 0.7, to transform from the Salpeter (1955) IMF they assumed to our assumed “diet Salpeter” IMF (see below). For the two ends of the cluster mass range considered above, the best-fit relations of Giodini et al. (2009) then give $M_{\text{gas}}/M_{*,0}$ of about 7 and 11, respectively. Finally, a recent analysis by Andreon (2010) of 52 clusters, chosen to have accurate measurements, results in similar relations, with values of $M_{\text{gas}}/M_{*,0}$ of about 7 and 13.5 for the two typical cluster masses, respectively.

Considering all of the above studies, we see that the estimates of $M_{\text{gas}}/M_{*,0}$ are in the range of 6 – 10 for the lower-mass clusters of the type monitored by most of the low- z surveys whose SN rates we analyze, 11 – 21 for the massive, intermediate- z clusters monitored by Gal-Yam et al. (2002) and by Sharon et al. (2010), and somewhere inside this range for the high- z cluster sample of Barbary et al. (2010). (We also note that these ratios appear to be independent of redshift; e.g. Giodini et al. 2009). When considering the iron mass in clusters and the number of SNe Ia needed to produce it, we therefore choose $M_{\text{gas}}/M_{*,0} = 10$ as our “optimal” fiducial value, but we will also consider the consequences of a “minimal iron” value of $M_{\text{gas}}/M_{*,0} = 6$.

3.3. The cluster iron abundance

A “canonical” value of $Z_{\text{Fe,gas}} = 0.3$ is by now fairly well-established for the ICM gas iron abundance, relative to solar. Balestra et al. (2006), Maughan et al. (2008), and Anderson et al. (2009) argue for values that have evolved even higher, to 0.4 – 0.5, at low redshifts (but see Ehlert & Ulmer 2009). To err conservatively, we adopt $Z_{\text{Fe,gas}} = 0.3$ for our fiducial value. These iron abundances typically relate to the central ~ 1 Mpc radius of massive clusters, the same region in which the stellar luminosity is measured and the SNe are detected by the cluster SN surveys we consider. Nevertheless, because the X-ray emission is strongly centrally peaked, there is some concern that the above iron abundance could be strongly biased by a high abundance in the very core region, which might be unrepresentative of a much lower abundance existing over most of the volume within 1 Mpc. However, Maughan et al. (2008) have shown that measuring iron abundances within an annulus that excludes the central 15% in radius reduces the results only mildly, to values still consistent with the canonical $Z_{\text{Fe,gas}} = 0.3$. For the stellar iron abundance relative to solar, we follow Maoz & Gal-Yam (2004) and

Lin et al. (2003) in adopting the value $Z_{\text{Fe,*}} = 1.2$ from the study by Jorgensen et al. (1996).

3.4. The CC SN contribution

$M(> 8M_{\odot})/M_{*,0}$ is the ratio between the initial mass in stars of mass above $8M_{\odot}$, which will explode as CC SNe, and the present-day mass in stars in clusters. Maoz & Gal-Yam (2004) examined the dependence of this ratio on the choice of IMF for a large range of standard and non-standard IMFs. In the present work, we will consistently assume the “diet Salpeter” IMF of Bell et al. (2003), as this is the IMF that has been assumed when determining rates per unit mass in the SN surveys that we analyze. This IMF is like the Salpeter (1955) single-power-law IMF with slope -2.35 between 0.1 and $100M_{\odot}$. However, when calculating observables involving mass, such as M/L , the total initial mass in stars is scaled down by a factor of 0.7, to simulate the deficit, relative to the Salpeter IMF, of low-mass stars in realistic IMFs. The ratio of mass in stars of mass above $8M_{\odot}$ to the total initial mass, in such an IMF, is 0.20. From Bruzual & Charlot (2003), for a Salpeter (1955) IMF, during the stellar evolution of a 10 Gyr-old population 31% of the stellar mass is returned to the interstellar medium (ISM) via stellar winds and SN explosions. For a diet Salpeter IMF, this mass-loss fraction is $0.31/0.7 = 44\%$, and hence the present-day ratio $M(> 8M_{\odot})/M_{*,0} \approx 0.2/0.56 = 0.35$. This is, in the present context, a conservative estimate, in that it maximizes the contribution of CC SNe, relative to SNe Ia, to cluster iron production. If, as generally believed, stars in some mass ranges collapse directly into black holes, without a SN explosion and its contribution to iron production, then the appropriate mass ratio to be used here would be lower. For example, if only stars up to $50M_{\odot}$ or $25M_{\odot}$ explode as CC SNe, $M(> 8M_{\odot})/M_{*,0}$ will be reduced to 0.29 or 0.20, respectively.

The diet Salpeter IMF gives a very similar $M(> 8M_{\odot})/M_{*,0}$ ratio to that of the Kroupa (2001) and Gould et al. (1997) IMFs (see Maoz & Gal-Yam 2004 and Bell et al. 2003). In any case, since both the SN rate and the iron mass in clusters are normalized relative to stellar mass, as derived from observed stellar luminosity, the conclusions are insensitive to the assumed form of the IMF in the low-mass range, as long as it is assumed consistently for both. The ratio $M(> 8M_{\odot})/M_{*,0}$ also depends weakly on the assumed age of the population, as long as it is of order several Gyr or more, since most of the return of mass to the ISM occurs early on.

Finally, we follow Maoz & Gal-Yam (2004) in assuming that the iron yield of a CC SN, y_{cc} , is 1% of the initial mass of the progenitor star. As discussed there, this is likely to be a conservative overestimate as well. For $M(> 8M_{\odot})/M_{*,0} = 0.35$ and the fiducial values of the metallicities, this means about 1/3 of the cluster iron mass was produced by CC SNe. For $M(> 8M_{\odot})/M_{*,0} = 0.20$, less than 1/5 of the iron mass is from CC SNe. Alternatively, for the “minimal iron” value of $M_{\text{gas}}/M_{*,0} = 6$, the core-collapse contribution is between 1/2 and 1/4.

3.5. The SN Ia iron yield and correction for stellar mass evolution

Dividing Eq. 1 by the mean iron yield of SNe Ia gives the time-integrated number of SNe Ia that have exploded in clusters, per present-day unit stellar mass, $N_{\text{SN}}/M_{*,0}$. The mean iron yield of a SN Ia is $0.6 - 0.7 M_{\odot}$ (e.g., Mazzali et al. 2007). In line with our conservative approach, we will assume the higher value of $0.7 M_{\odot}$, thus lowering the integrated number of SNe Ia required to explain the observed abundances.

The time-integrated number of SNe Ia per unit *formed* stellar mass, before the 44% mass loss that occurs over the course of ~ 10 Gyr (see §3.4, above), will be 0.56 times lower. Multiplying Eq. 1 by $0.56/0.7M_{\odot}$, we thus obtain the time-integrated number of cluster SNe Ia per unit formed stellar mass,

$$\left(\frac{N_{\text{SN}}}{M_*}\right)_{\text{opt}} = 0.0059 M_{\odot}^{-1} = 5.9 \text{ SNuM Gyr}, \quad (2)$$

assuming the “optimal” value of $M_{\text{gas}}/M_{*,0} = 10$, and the other fiducial values in Eq. 1. Alternatively, for the “minimal” value of $M_{\text{gas}}/M_{*,0} = 6$, we obtain

$$\left(\frac{N_{\text{SN}}}{M_*}\right)_{\text{min}} = 0.0034 M_{\odot}^{-1} = 3.4 \text{ SNuM Gyr}, \quad (3)$$

4. A RECONSTRUCTION OF THE OBSERVATIONAL SN DELAY-TIME DISTRIBUTION

In this section, we combine the observed cluster SN rates, $R_{\text{Ia}}(t)$ (from §2) and the integrated SN Ia number per formed stellar mass, N_{SN}/M_* (from §3), to recover the SN Ia DTD. In the next section, we take an alternative, forward-modeling, approach, to examine the predictions of a variety of specific model DTDs. Throughout this section, we assume that all stars in clusters formed in a single instantaneous burst, neglecting any subsequent star formation. As already noted above, this is a fair approximation to the results of spectral synthesis of the mass-dominant stellar populations in cluster ellipticals, indicating a burst lasting ~ 0.1 Gyr at $z_f \approx 3$ (corresponding to cosmic time $t_f \approx 2$ Gyr), i.e., some 11.5 Gyr ago. The consequences of relaxing the instantaneous-burst assumption are studied in §6-7, below. If, in fact, the burst assumption is valid, recovery of the DTD is straightforward. The SN rate since the epoch of star formation differs from the DTD only in the stellar-mass normalization – the DTD is the SN rate normalized by unit stellar mass at the formation epoch, M_* , while the SN rate is normalized by the remaining stellar mass, $M_*(t) = M_* m(t)$, at the cosmic epoch of the rate measurement. Here, $m(t)$ is the remaining fraction of the initially formed stellar mass at cosmic time t (since the Big Bang). The observed SN rates per unit mass at cosmic times t are the values of the DTD at delays $t - t_f$, up to the correction, easily applied, to convert from the existing mass at time t to the formed mass at t_f , accounting for mass loss during stellar evolution. The SN rate and the DTD are thus related by

$$R_{\text{Ia}}(t) = \frac{\Psi(t - t_f)}{m(t - t_f)}. \quad (4)$$

Bruzual & Charlot (2003) tabulate the relative accumulated stellar mass loss versus time, $m_{\text{loss}}(t)$, following a burst of star formation, assuming a Salpeter (1955) IMF. For the “diet Salpeter” IMF, the remaining mass

fraction is $m(t) = 1 - m_{\text{loss}}(t)/0.7$. Starting 2.5 Myr after star formation, the remaining mass $m(t)$ is well approximated as $(t/2.5 \text{ Myr})^{-0.07}$. The predicted SN rate will therefore decline slightly less steeply than the DTD. We convert the observed SN rates, R_{Ia} , to the DTD, $\Psi(t)$, using Eq. 4 with the full Bruzual & Charlot (2003) mass loss (rather than the power-law approximation).

To estimate the DTD at delay times earlier than those corresponding to the redshift, z_{max} , of the most distant clusters monitored, we can use the N_{SN}/M_* constraints from the iron observations. The total number of SNe per unit formed stellar mass between z_f and z_{max} is $(N_{\text{SN}}/M_*)_{z_f, z_{\text{max}}} = (N_{\text{SN}}/M_*) - (N_{\text{SN}}/M_*)_{z_{\text{max}}, 0}$, where $(N_{\text{SN}}/M_*)_{z_{\text{max}}, 0}$ is the total number between $z = 0$ and z_{max} , obtained by integrating the DTD over that range. The mean DTD value in the time interval $[0, t_{\text{max}} - t_f]$, corresponding to the unobserved redshift range z_f to z_{max} , is just $(N_{\text{SN}}/M_*)_{z_f, z_{\text{max}}}/(t_{\text{max}} - t_f)$.

To estimate $(N_{\text{SN}}/M_*)_{z_{\text{max}}, 0}$, we integrate, using small time steps, over the mass-loss-corrected SN rates. At times that are covered by several measurements, we take a mean rate, weighted by the relative measurement errors. Out to $z = 1.45$, we find an integrated SN to stellar mass ratio of $(N_{\text{SN}}/M_*)_{z_{\text{max}}, 0} = 8.2 \times 10^{-4} M_{\odot}^{-1}$. Subtracting this from the minimal-iron value of $0.0034 M_{\odot}^{-1}$ (Eq. 3) leaves $0.0026 M_{\odot}^{-1}$ in the time interval of 2.2 Gyr between $z_f = 3$ to $z_{\text{max}} = 1.45$, or a mean DTD value of $0.012 \text{ SNe yr}^{-1}(10^{10} M_{\odot})^{-1}$ in this delay time interval of $0 - 2.2$ Gyr. For the optimal-iron value (Eq. 2) of $0.0059 M_{\odot}^{-1}$, the mean DTD value in this time bin is $0.023 \text{ SNe yr}^{-1}(10^{10} M_{\odot})^{-1}$. We take this range of DTD values as the uncertainty, which is driven in this case mainly by the systematic uncertainty in the cluster gas-to-stellar mass ratio. For our best estimate we take the optimal-iron value. We note that this exercise implies that, for the minimal and optimal iron assumptions, respectively, 79% to 88% of the SNe Ia in clusters exploded before $z = 1.45$.

Figure 2 shows the recovered DTD, whose values are also listed in Table 1. The horizontal error bars mark the limits of each DTD time bin, while the vertical error bars show the summed (not in quadrature) and propagated statistical and systematic errors. Also shown in Fig. 2 are three other recently recovered observational SN Ia DTDs. One (empty circles) is from Maoz et al. (2010), obtained for a subsample of the local galaxies in the Lick Observatory SN Search having individual SFH reconstructions based on SDSS spectra. We have plotted here the Maoz et al. (2010) DTD from a subsample that excluded galaxies of Hubble types Sa to Sbc, in order to reduce cross talk between time bins. Due to the limited aperture of the SDSS spectrograph fibers, there remains a “leak” of signal from the first to the second time bins, and therefore the plotted DTD level in the $40 - 420$ Myr time bin is likely an underestimate of the true level (see Maoz et al. 2010). Another DTD shown (empty triangles) was found by Maoz & Badenes (2010), using the SN remnants in the Magellanic Clouds as an effective SN survey. In this DTD, there is a detection in one time bin, of $t < 330$ Myr, but only an upper limit on the DTD value between 330 Myr to a Hubble time, which is indicated. Finally, we show (empty squares) the DTD recovered by Totani et al. (2008), using SN Ia can-

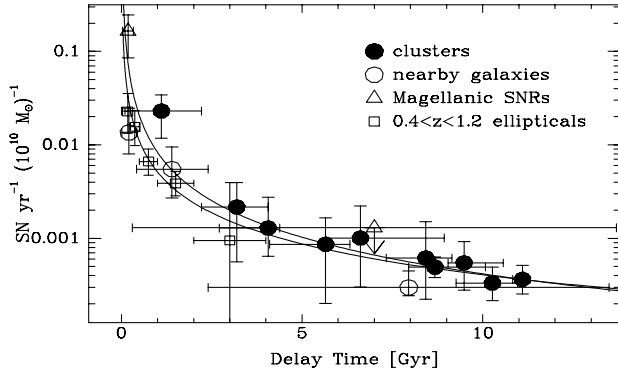


FIG. 2.— Recovered SN Ia delay-time distribution (DTD) for galaxy clusters (filled circles). All but the earliest point are obtained directly from the observed rates in Fig. 1, after correcting them for stellar mass loss, and assuming an instantaneous star-formation burst at $z_f = 3$ for all clusters. Horizontal error bars indicate the time bin over which each mean DTD value is evaluated. The first point is obtained by requiring a time-integrated number of SNe Ia according to Eqns. 2-3, satisfying the observed iron-to-stellar mass ratio in clusters. Also plotted, for comparison, are the recovered observational DTDs from: Maoz et al. (2010), based on SNe in nearby galaxies from LOSS (empty circles); Maoz & Badenes (2010), based on SN remnants in the Magellanic Clouds (empty triangles, with arrow marking the 95% confidence upper limit); and Totani et al. (2008) based on SN Ia candidates in elliptical galaxies at $z = 0.4 - 1.2$ (empty squares). For reference, we also show (curves) power laws, t^{-s} , with $s = -1.1$ and $s = -1.3$, scaled to pass through the latest cluster-based point.

didates in SXDS field elliptical galaxies at $z = 0.4 - 1.2$. We have divided the DTD values of Totani et al. by a factor 1.8, given by them, to convert from their normalization unit, of present-day K -band luminosity, to ours, of formed stellar mass. We have then divided by a further factor 0.7 to convert from their assumed Salpeter (1955) IMF to our diet-Salpeter IMF. We also show, for reference, two power laws, $\Psi \propto t^{-1.1}$ and $\Psi \propto t^{-1.3}$, which are discussed further in § 5.1, below.

Several facts are apparent in Fig. 2. First, considering the different time bins of the different measurements, and the known systematics, the various measurements are generally consistent with each other in regions of overlap. Second, the DTD is a monotonically decreasing function, peaking at the earliest delays probed by the observations. Finally all the plotted points appear to be generally consistent with the illustrated power-law dependences, which, remarkably, pass through each and every error box. This consistency is tested quantitatively in § 5.1. With this new DTD derivation, combined with those by Maoz et al. (2010) and Maoz & Badenes (2010), we thus confirm and extend the results of Totani et al. (2008), who found in their field elliptical SN sample a best-fit DTD dependence of a power law, $\Psi \propto t^s$, with $s = 1.08 \pm 0.15$. This is also further discussed below, in § 5.1.

5. COMPARISON TO DTD MODELS – SINGLE-COMPONENT MODELS

In this section, we take a forward-modeling approach, to compare the predictions of specific model DTDs to the observations. Forward modeling is advantageous in that the actual data are not manipulated and errors need not

be propagated. Furthermore, this approach will permit us later (§6-7) to relax the assumption of a single short burst of star formation in clusters.

A model DTD that we test, $\Psi(t)$, in order to be consistent with observed cluster iron abundances, needs to have a normalization such that its integral over a cluster stellar age, t_0 , agrees with the above, time-integrated, SN numbers:

$$\int_0^{t_0} \Psi(t) dt = \frac{N_{\text{SN}}}{M_*}. \quad (5)$$

This is one constraint on the DTD, imposed by the cluster iron abundances. A second set of constraints is imposed by the observed time dependence of the SN rate, which can be compared to the model DTD predictions. The predictions will be tested with the χ^2 figure of merit. The SN rate at each visibility-time-weighted mean redshift is compared with the model prediction, with the latter averaged over the redshift interval spanned by the cluster sample used for deriving each SN rate. Errors on the observed rates are generally asymmetric. For the χ^2 calculation, we use the error that is on the model side of each data point.

Throughout this section, we assume that all stars in clusters formed in a single instantaneous burst, neglecting any subsequent star formation. As already noted above, this is a fair approximation to the results of spectral synthesis of the mass-dominant stellar populations in cluster ellipticals, indicating a short burst at $z_f \approx 3$. As noted in §4, the SN rate since the epoch of star formation differs from the DTD only in the stellar-mass normalization, whether formed mass, M_* , or remaining stellar mass, $M_*(t) = M_* m(t)$, at the epoch of the rate measurement, and we again use Eq. 4, this time to convert the DTD model, $\Psi(t)$, to a rate prediction, $R_{\text{Ia}}(t)$.

Various forms have been proposed for the DTD, some derived from detailed binary population synthesis calculations (e.g., Yungelson & Livio 2000; Han & Podsiadlowski 2004; Ruiter et al. 2009; Bogomazov & Tutukov et al. 2009; Mennekens et al. 2010); some physically motivated mathematical parameterizations, with varying degrees of sophistication (e.g., Madau et al. 1998; Greggio 2005; Totani et al. 2008); and some ad hoc formulations intended to reproduce the observed field SN rate evolution (e.g., Strolger et al. 2004). We now attempt to fit the observed cluster SN Ia rates with some of these proposed DTDs, using Eq. 4, while simultaneously satisfying the DTD normalization constraint, Eq. 5, set by the iron abundances in clusters.

5.1. Power-law DTDs

A first and simple mathematical parametrization of the DTD that we compare to the observed cluster SN rates is a power law in time, $\Psi(t) \propto t^s$. Power laws have been long considered as possible forms of the DTD (e.g., Ciotti et al. 1991; Sadat et al. 1998). As noted by previous authors (e.g., Greggio 2005; Totani et al. 2008) a power-law dependence is generic to models (such as the DD model) in which the event rate ultimately depends on the loss of energy and angular momentum to gravitational radiation by the progenitor binary system. If the dynamics are controlled solely by gravitational wave losses, the time t until a merger depends on the binary

separation a as

$$t \sim a^4. \quad (6)$$

If the separations are distributed as a power law

$$\frac{dN}{da} \sim a^\epsilon, \quad (7)$$

then the event rate will be

$$\frac{dN}{dt} = \frac{dN}{da} \frac{da}{dt} \sim t^{(\epsilon-3)/4}. \quad (8)$$

For a fairly large range around $\epsilon \approx -1$, which describes well the observed distribution of initial separations of non-interacting binaries (see Maoz 2008 for a review of the issue in the present context), the DTD will have a power-law dependence with index not far from -1 . However, in reality, the binary separation distribution of WDs that have emerged from their common envelope phase could be radically different, given the complexity of the physics of that phase. Thus, the $\sim t^{-1}$ DTD dependence of the DD channel cannot be considered unavoidable. Be that as it may, the DTD reconstructions by Totani et al. (2008), Maoz et al. (2010), Maoz & Badenes (2010), and in this work (§4), all point to a $\sim t^{-1}$ power-law.

A different power-law DTD dependence, with different physical motivation, has been proposed by Pritchett et al. (2008). If the time between formation of a WD and its explosion as a SN Ia is always brief compared to the formation time of the WD, the DTD will simply be proportional to the formation rate of WDs. Assuming that the main-sequence lifetime of a star depends on its initial mass, m , as a power law,

$$t \sim m^\delta, \quad (9)$$

and assuming the IMF is also a power law,

$$\frac{dN}{dm} \sim m^\lambda, \quad (10)$$

then the WD formation rate, and hence the DTD, will be

$$\frac{dN}{dt} = \frac{dN}{dm} \frac{dm}{dt} \sim t^{(1+\lambda-\delta)/\delta}. \quad (11)$$

For the commonly used value of $\delta = -2.5$ and the Salpeter (1955) slope of $\lambda = -2.35$, the resulting power-law index is -0.46 , or roughly $-1/2$. Pritchett et al. (2008) have argued that such a $t^{-1/2}$ form for the DTD can explain the trend of SN Ia rate versus specific star-formation rate of the host population in the Supernova Legacy Survey.

We test model power-law DTDs with these two particular power-law indices, -1 , and $-1/2$, as well as a continuous range of indices, s , against the cluster data. We assume $\Psi(t) = 0$ for $t < 40$ Myr, corresponding to the lifetime of $8M_\odot$ stars (e.g., Girardi et al. 2000), at the border between CC and WD formation. We start by setting the star-formation redshift at $z_f = 3$, i.e., at a cosmic time $t_f = 2.1$ Gyr.

Fitting the observed cluster SN rates with a power law DTD having a free normalization and index s , the best fit is obtained for $s = -1.2$. The time-integrated SN number is $N_{\text{SN}}/M_* = 0.0044$ for a power law of this slope, which is intermediate to the “minimal iron” value we have derived above (Eq. 3) and the “optimal” value

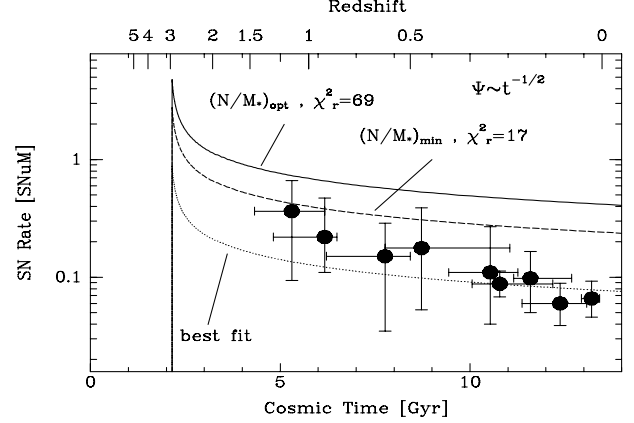


FIG. 3.— Fits of the predictions of $\Psi \propto t^{-1/2}$ power-law DTDs to the observed cluster SN Ia rates, plotted as a function of time since the Big Bang, assuming instantaneous cluster star formation at $z_f = 3$, and SN Ia events starting 40 Myr after star formation. The best-fitting version (dotted curve) has a time-integrated number of SNe that is only a minor fraction of that required to produce observed cluster iron-to-stellar mass ratios. Versions scaled to produce the minimal (dashed curve) or optimal (solid curve) integrated number of SNe give poor fits to the cluster rates, with the reduced χ^2 values indicated.

(Eq. 2). However, with the normalization thus unconstrained, χ^2 depends weakly on s , and there is a wide range of indices, $-1.6 < s < 2.7$, that give acceptable fits to the observed rates. (We will deem as “acceptable” those model with $\chi^2_r < 2$, which corresponds to a probability of $> 5\%$ for 7 d.o.f. – 9 data points minus two free parameters, s and the normalization.) The steeper ones among these power laws also have sufficiently large integrals. Specifically, power laws with $s < -0.88$ satisfy the minimal iron constraint, while shallower power laws, e.g., $s = -0.5$, do not.

Conversely, an $s = -0.5$ power-law normalized to have the correct integral, when compared to the data, grossly overpredicts the observed rates, giving an unacceptably high reduced chi-square, $\chi^2_r = \chi^2/\text{d.o.f.}$, of 17 and 69 per degree of freedom (d.o.f.), for the minimal and optimal normalizations, respectively. (In the latter two fits, there are no free parameters that are adjusted to fit the data, and hence we have 9 degrees of freedom, as the number of independent data points.) Figure 3 shows these three fits. Thus, a $t^{-1/2}$ power law, while it can describe well the time dependence of the cluster rates at $0 < z < 1.45$, cannot simultaneously produce the required time-integrated SN Ia numbers.

If we force the minimal-iron constraint, the best-fit power law is $t^{-1.1}$, with an acceptable $\chi^2_r = 0.11$, as shown in Fig. 4. The low χ^2 value indicates that the errors on at least some of the rates have been conservatively overestimated. The combined constraints of the SN rate data and the minimal iron abundances limit the acceptable values of the power law index to $s = -1.10^{+0.28}_{-0.22}$. For the optimal iron constraint, the acceptable range of indices is $s = -1.28^{+0.25}_{-0.18}$, with $\chi^2_r = 0.10$ for the best fit. Smaller, more realistic, rate uncertainties would reduce these allowed ranges.

We thus see that a simple parametrized model DTD of the form t^{-1} , or slightly steeper, can provide a good fit to the cluster SN Ia rates while simultaneously providing

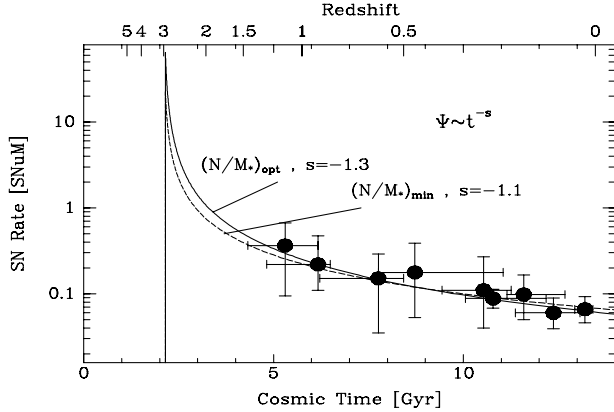


FIG. 4.— Same as Fig 3, but for steeper power law DTDs, $\Psi \propto t^{-s}$, with $s = -1.1$ and the minimum-iron normalization (dashed curve), and $s = -1.3$ plus the optimal-iron normalization (solid curve). In both cases, there is a good fit to the cluster SN rate data.

a sufficient time-integrated number of SNe Ia to satisfy the iron-based constraints.

We note that these conclusions depend weakly on the chosen epoch of cluster star formation, t_f . For a given power-law slope, acceptable fits are obtained for t_f in the range 1.2 to 2.3 Gyr, corresponding to $z_f = 4.8$ to 2.8, with a best fit that has a constant minimum χ^2 in the range $z_f = 3.2 - 3.7$. Varying t_f cannot salvage power-law DTDs such as $t^{-1/2}$, that are strongly ruled out because of the shallowness of their slope. However, moving t_f back can slightly increase the allowed range of slopes. For example, for the optimal iron value, the maximal acceptable power-law slope can be raised from -1.11 to -1.08 by shifting z_f back to 3.6.

It is arguable that, instead of a single, $\sim t^{-1}$ power law, motivated by binary mergers, with this power law extending back to delays as short as 40 Myr, there could be a “bottleneck” in the supply of progenitor systems below some delay. Such a bottleneck could be due to the birth rate of WDs, which behaves as $\sim t^{-1/2}$. One possible result would then be a broken-power-law DTD, with $\Psi \propto t^{-1/2}$ up to some characteristic time, t_c , and $\Psi \propto t^{-1}$ thereafter. A possible value could be $t_c \approx 400$ Myr, corresponding to the lifetimes of $3M_\odot$ stars. If that were the lowest initial mass of stars that can produce the WD primary in a DD SN Ia progenitor, then beyond t_c the supply of new systems would go to zero, and the SN Ia rate would be dictated by the merger rate.

We have therefore attempted to fit the data with such a $t^{-1/2}$, t^{-1} broken power law. With the DTD normalization fixed to produce the required minimum iron integrated SN numbers, this model gives an acceptable $\chi_r^2 = 1.2$, though this is considerably worse than the single power-law fit, and could become unacceptable with more realistic errors. We test the optimal iron value with a $t^{-1/2}$, $t^{-1.3}$ broken power law, that is steeper at late times (since even t^{-1} alone is already rejected, see above). Here, too, an acceptable $\chi_r^2 = 0.9$ is found. For the minimal-iron normalization, a $t^{-1/2}$, $t^{-1.1}$ dependence is acceptable, as long as $t_c < 1.5$ Gyr. Such a late break time is interesting in the context of sub-Chandra

merger models, in which the mergers of white dwarfs of initial masses smaller than $3M_\odot$ produce SNe Ia (Sim et al. 2010; Van Kerkwijk et al. 2010).

To summarize, the cluster SN rates plus iron abundances can be fit with a power-law DTD, under some conditions. Assuming the minimal iron mass value indicated by cluster observations, a range of slopes with values of $s \approx -1$, or somewhat steeper, is allowed. A break to a shallower $t^{-1/2}$ dependence at $t < t_c$ is also permitted, provided the power-law is steep enough at longer delays, and the break does not occur too late. For the acceptable range of power-law DTDs, between 50% and 85% of SNe Ia explode during the first Gyr after star formation.

5.2. DTDs from binary population synthesis models

Over the past decade, a number of groups (e.g., Yungelson & Livio 2000; Han & Podsiadlowski 2004; Belczynski et al. 2008; Ruiter et al. 2009; Bogomazov & Tutukov 2009; Wang, Li, & Han 2010; Mennekens et al. 2010) have calculated DTDs using binary population synthesis (BPS), in which a large number of binaries with a chosen distribution of initial conditions are followed through the stages of stellar and binary evolution, to the point that some of them reach the conditions for explosion as SNe Ia. In our comparison to cluster SN rates, we focus here, as examples, on the models presented by Yungelson & Livio (2000), and on the more recent ones by Mennekens et al. (2010). As opposed to the simple parametrized models, considered above, the BPS models can make absolute predictions of SN rates vs. time, i.e., their normalizations are set. Therefore, in our comparisons of these models to the observed rates and to the integrated iron mass in clusters, we first consider the “raw” predictions of the models, without any scalings, and then proceed to test scaled versions.

Yungelson & Livio (2000) studied four different evolutionary paths to a SN Ia: a DD model; an SD model with accretion of He from a giant companion and detonation at sub-Chandrasekhar mass, through an edge-lit detonation caused by ignition of the He layer (He-ELD); and SD models with accretion from a sub-giant companion and detonation at the Chandrasekhar mass (SG-Ch), or through an edge-lit detonation (SG-ELD). The DTDs for these different paths can be seen in their fig. 2. We have scaled up these DTDs by a small factor of 1.05, to convert from the IMF assumed by Yungelson & Livio (2000) to our adopted diet Salpeter IMF. Their assumed IMF is a broken power law, of index $\lambda = -2.5$ from $0.3M_\odot$ to $100M_\odot$, and with $\lambda = 0$ from $0.08M_\odot$ to $0.3M_\odot$ (L. Yungelson, private communication). (For a fully self-consistent comparison of the shapes of the DTDs, their models would need to be re-calculated with our adopted IMF, but it is unlikely that the different IMF slopes, -2.5 and -2.35 , over the limited range of masses that contribute to SN Ia progenitors, would lead to major changes in the DTD). Two of the models, He-ELD and SG-Ch, predict no SNe beyond 1.5 – 2 Gyr after star formation, where all the measured cluster SN rates are. These models are obviously inconsistent with the observed rates, although they could play a role in a multi-component DTD scenario (see §7, below). The DD and SG-ELD models, on the other hand, do predict SN

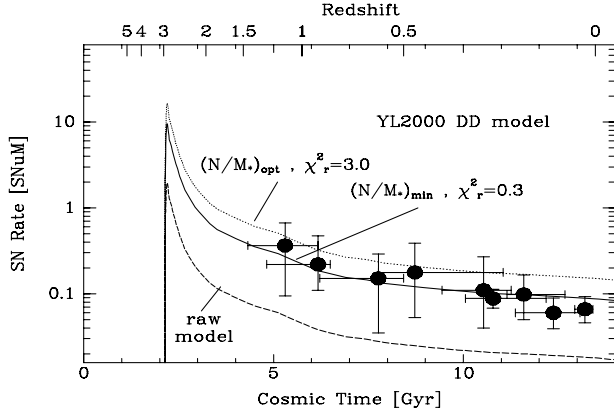


FIG. 5.— Comparison of the observed cluster SN rates to the predictions of the DD model from the BPS simulations of Yungelson & Livio (2000). The “raw” prediction of the model (dashed curve), without any scaling, underpredicts both the observed rates and the required integrated number by a factor of 5. A version of the model (solid line) scaled to produce the minimal-iron normalization matches well the observed rates. When scaled to the optimal-iron value, however, it overpredicts the low-redshift cluster rates.

events on long time scales, and can be tested.

Figure 5 compares the predictions of the DD model of Yungelson & Livio (2000) to the observations. The “raw” version of this model, without any re-scaling of the DTD (beyond the adjustment above for conversion between the IMFs), underpredicts the observed cluster SN rates, with a poor $\chi^2_r = 2.9$. Its integrated number of SNe per formed stellar mass is $N_{\text{SN}}/M_* = 0.0007$, just 1/5 of the minimal-iron value, and only 12% of the optimal value. This confirms previous assertions by Maoz (2008), Ruiter et al. (2008), and Mennekens et al. (2010), that BPS models underpredict observed SN rates by at a factor of at least a few, and likely by more. As seen in Fig. 5, if we scale up the model by a multiplicative factor of 5, so as to integrate to the minimal-iron value, we obtain an acceptable $\chi^2_r = 0.3$ for the rates. Although BPS models have many free parameters, it is not clear that such a level of scaling-up of the model could be achieved easily. If we force the DTD integral to the optimal-iron value, the predicted rates are too high, giving an unacceptable $\chi^2_r = 3.0$.

Proceeding to the SG-ELD model of Yungelson & Livio (2000), this model (Fig. 6) always gives a poor fit to the SN rates, whether in its raw form (which again produces only 23% of the minimum iron value), or scaled to satisfy the iron constraints, or even if scaled arbitrarily. The SG-ELD model begins making SNe Ia only about 800 Myr after star formation, and thus misses the opportunity of producing the bulk of the iron mass during that time. Furthermore, this model then predicts SN rates that fall too steeply with time. These problems cannot be alleviated by a change in the star-formation epoch, t_f , which has little effect on the fits, as was the case for parametrized power-law DTDs.

We turn now to the BPS models of Mennekens et al. (2010), who have examined both DD and SD models. They have assumed a Kroupa et al. (1993) IMF, consisting of a three-part broken power law, with index $\lambda = -1.3$ from $0.08M_\odot$ to $0.5M_\odot$, $\lambda = -2.2$ from $0.5M_\odot$ to $1M_\odot$, and $\lambda = -2.7$ from $1M_\odot$ to $100M_\odot$. The mass

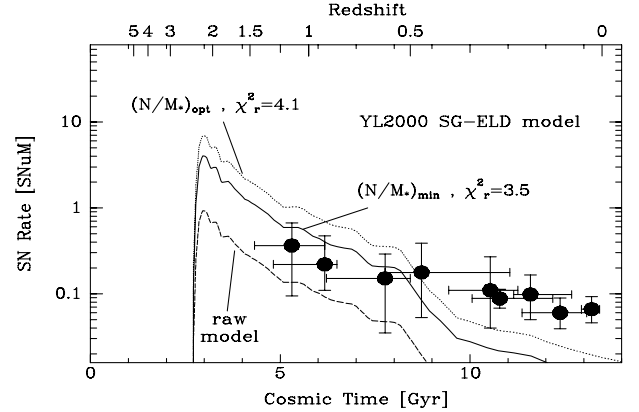


FIG. 6.— Same as Fig. 5, but for the SD model of Yungelson & Livio (2000) involving a sub-giant donor and an edge-lit detonation. The cluster epoch of star formation, as before, is assumed to be $z_f = 3$, but in this model the first SN Ia events are delayed by ~ 800 Myr. Because of the steep decline of this model DTD, neither the raw models, nor those scaled to the normalizations required by iron abundances, match the rate observations.

ratio between this IMF and the diet-Salpeter IMF is 0.92, and we therefore scale down the Mennekens et al. (2010) DTDs by this factor.

In their DD models that we examine, Mennekens et al. (2010) introduce the possibility of non-conservative Roche-lobe overflow, which they parametrize with a β parameter, the fraction of material lost by the donor star that is accepted by the accreting star. Values of $\beta = 0, 0.8, 0.9$, and 1.0 are considered. The α parameter (Webbink 1984), which is the fraction of the orbital energy lost during the common-envelope phase that is transferred to kinetic energy of the envelope, is set to 1. An additional DD model is calculated with $\beta = 1$, but treating the common-envelope phase, instead of with the α model, by using the γ parametrization of Nelemans & Tout (2005), with $\gamma = 1.5$. The γ approach quantifies the change in angular momentum during the common envelope phase. Two SD models with $\beta = 1$ have also been calculated by Mennekens et al. (2010), one with $\alpha = 1.0$ and one with $\gamma = 1.5$.

Fitting these models to the cluster rates, with or without the cluster iron constraints, we find the following. None of the raw DTDs of Mennekens et al. (2010) produce enough time-integrated SN numbers to reproduce the observed iron abundances. At best, the $\beta = 0.8$ and $\beta = 0.9$ DD models produce 12% of the minimal-iron value, and the SD $\alpha = 1$ model makes 16%. The other models make only a few percent or less of the minimal number of SNe required by cluster abundances. If we scale up the models, forcing the minimal-iron normalization, the Mennekens et al. (2010) SD models, qualitatively like the Yungelson & Livio (2000) SD models discussed above, predict no SNe 4–5 Gyr after star formation, and hence cannot match the observed cluster rates. This is illustrated in Fig. 7. Two of the scaled Mennekens et al. (2010) DD models give acceptable fits to the observed cluster SN rates: DD with $\alpha = 1$ and $\beta = 0.9$; and DD with $\gamma = 1.5$ and $\beta = 1$. These fits are shown in Fig. 8.

To summarize our analysis of BPS models from these two teams, the emerging picture is that SD models al-

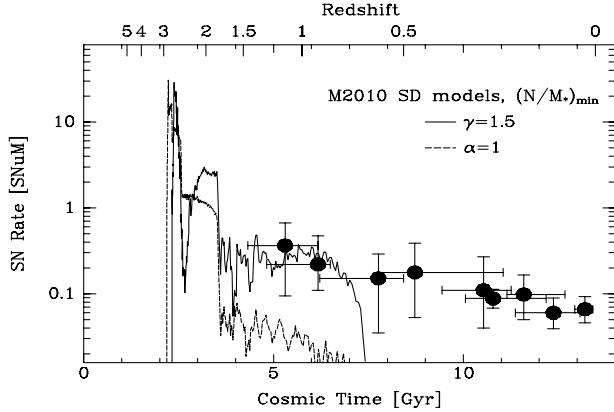


FIG. 7.— Rate predictions based on DTDs from two SD models by Mennekens et al. (2010), based on two different parametrizations of the physics of the common-envelope phase (see text). The models have been scaled up by factors of 80 ($\gamma = 1.5$ model, solid curve) and 6.4 ($\alpha = 1.0$ model, dashed curve), to match the minimal-iron constraint but both fall too steeply to match the observed cluster SN rate redshift dependence.

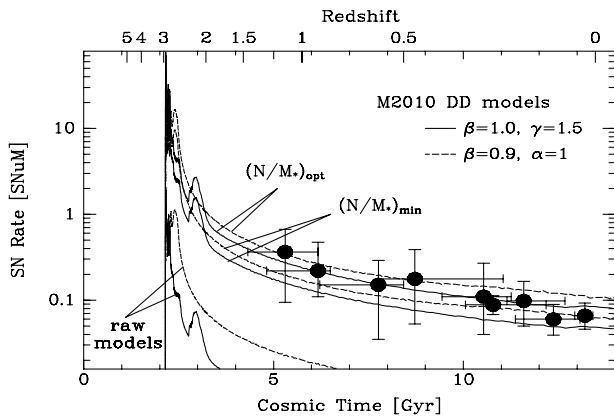


FIG. 8.— Same as Fig. 5, but for two of the DD models from the BPS calculations of Mennekens et al. (2010) that can match the data, if the raw DTDs are suitably scaled up according to the optimal iron requirement, or the minimal requirement, as marked. The parameter β quantifies the degree of mass conservation during the Roche-lobe overflow phase.

ways fit the observations poorly – in terms of both the absolute “raw” numbers of SNe they predict, and the time dependence of the cluster SN rates they predict. The raw DD models also underpredict the absolute SN numbers, but by lower factors, of 5 – 8. If we treat the BPS models as scalable, then for some of the DD models it is possible to simultaneously satisfy the minimal-iron constraints and the observed cluster SN rate dependence on redshift. The higher, optimal-iron, constraint can also be satisfied by two scaled DD models among those of Mennekens et al. (2010).

5.3. DTDs from analytical models

Another approach to making DTD predictions, followed by Greggio (2005), is to calculate analytical DTD models, based on stellar evolution arguments and on various parametrizations of the possible results of the complex common-envelope phases through which SN Ia progenitor systems must pass. For each of several SN Ia

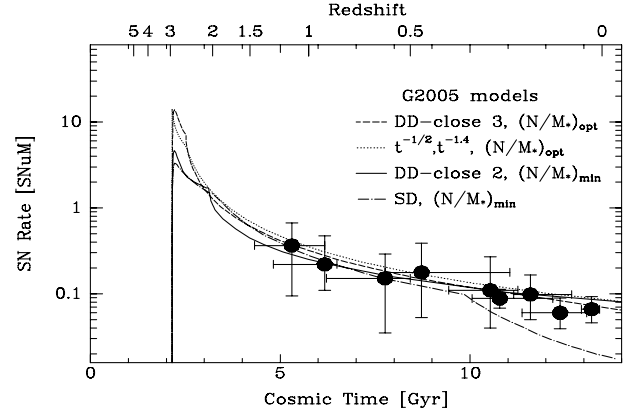


FIG. 9.— Comparison of the observed cluster SN rates to predictions by three of the analytic models of Greggio (2005), scaled to give either the minimal or optimal ratio of integrated SN numbers to stellar mass. The SD model, like the SD models from the BPS simulations, underpredicts the low- z cluster SN rate. Two of the DD models, however, can match the data. Also shown, for comparison (dotted line), is the prediction from a simple broken-power-law DTD: $t^{-1/2}$ at $40 \text{ Myr} < t < 400 \text{ Myr}$; $t^{-1.3}$ for $t > 400 \text{ Myr}$, having the minimal-iron normalization, which is similar to the DD-close-3 model (dashed curve).

channels, she calculated the DTDs that emerge when varying the values for the parameters describing the initial conditions, and the mass and separation distributions and limits of the systems that eventually explode. Mennekens et al. (2010) have criticized this approach in that it overlooks the changes in stellar-evolution timescales that occur as a result of the “rejuvenation” due to mass transfer between stars. On the other hand, an advantage of the analytic approach, compared to the BPS approach, is that predictions for a large range of parameters can be made quickly. This successful range can then be investigated in more detail with actual BPS simulations.

We focus on a selection of representative models shown in fig. 1 of Greggio et al. (2008). These include one SD model and four DD models, computed under different assumptions for these parameters. The “wide” and “close” labels of the DD models refer to two possible parametric schemes used by Greggio (2005) to describe the WD separation distribution after the common envelope phase. The Greggio models do not predict the absolute levels of the SN rates (i.e., the normalization of the model DTDs), as this is another free parameter in the models. We therefore examine only various scaled versions of the Greggio models.

The DD-close model with a minimum secondary initial mass of $3M_{\odot}$ fits the observed SN rate redshift dependence, while satisfying either the minimal iron constraint (with $\chi_r^2 = 0.52$) or the optimal iron constraint (with $\chi_r^2 = 0.45$). Maoz et al. (2010) have already noted the good agreement between this Greggio (2005) model and a DTD reconstructed from the SNe in the LOSS-SDSS subsample, and the fact that this Greggio model is similar to a $t^{-1/2}, t^{-1.3}$ broken power-law with break at $t_c < 400 \text{ Myr}$. Such a broken power law was shown to fit well the data and the minimal-iron constraint in §5.1, above. The resemblance is seen in Fig. 9. The DD-close model with a minimum secondary mass of $2M_{\odot}$, also shown in Fig. 9, can fit the rates as well, but only with the minimal-iron constraint, due to its shallower

slopes at both early and late times. The two DD-wide models of Greggio (2005) we test, with minimal masses of $2M_\odot$ and $2.5M_\odot$, are both too shallow to fit the rates and either of the normalizations, and give $\chi_r^2 > 3.6$.

Finally, the SD model of Greggio (2005), while having a DTD that is more extended in time than the SD models from BPS that we have examined above, suffers from similar problems, particularly a steep drop in rates beyond ~ 8 Gyr. The minimal-iron normalized SD model, shown in Fig. 9, is formally acceptable, with $\chi_r^2 < 2$, but its low predicted rates at low redshifts are in conflict with the measurements. (Poisson statistics would be more appropriate to compare the low prediction to the accurately measured, non-zero, rates at low redshift.)

Thus, only the two DD-close Greggio (2005) models are consistent with the rates and the iron data. This is simply the result of the fact that DD models generically produce power-law DTDs, and the power-laws required to fit simultaneously the observed rates and the normalizations need to have indices of ≈ -1 or steeper. Such indices can be obtained by emerging from the common-envelope phase with a steep power-law separation distribution, i.e., with relatively more close pairs, as discussed in §5.1 and seen in Eq. 8. Naturally, we have examined a limited range of the Greggio (2005) models, and it would be interesting to see if there are others (e.g. Greggio 2010) that do fit the data, and what are their parameters.

6. COMPARISON TO DTD PREDICTIONS – NON-INSTANTANEOUS CLUSTER STAR-FORMATION HISTORIES

So far, we have assumed the cluster SFH to be a single, instantaneous burst at z_f . We now test whether relaxing this assumption can improve the fit of any of the models to the data, in terms of reproducing both the time dependence of the SN Ia rate and the normalization, as required by the iron abundance. Furthermore, a non-instantaneous burst may be a more realistic description of cluster SFH. The predicted SN rate will now be a convolution of the SFH, $S(t)$, with the DTD, after correction for stellar mass loss,

$$R_{Ia}(t) \propto \int_0^t S(t-\tau) \frac{\Psi(\tau)}{m(\tau)} d\tau. \quad (12)$$

We consider a single, but non-instantaneous, burst of star formation in galaxy clusters in the form of an exponentially decaying SFH, $S(t) \propto \exp[-(t - t_f)/\tau_{SF}]$, starting at time t_f . More complex SFHs are considered in §7.2, below. We have re-fit the cluster rates with the iron-mass normalizations using all the DTD models discussed in §5, above, but convolved with this exponential SFH, with values of $\tau_{SF} = 0.5, 1, 2, 3, 4$ Gyr. The effect on the SN rate of the convolution between the DTD and any temporally extended star formation is always to transfer some fraction of the SN events to later times. Since all the DTDs that we consider peak at short delays, this means that the SN rate rises more slowly at early times than in the instantaneous burst approximation. This, in turn, means that a smaller fraction of the time-integrated SN number, dictated by the iron abundances, can be produced at early times. Raising the model normalization, such that the iron constraints are met, then results in a poor fit to the SN rate data, compared to the instantaneous case. To try to mitigate this effect, we shift back by

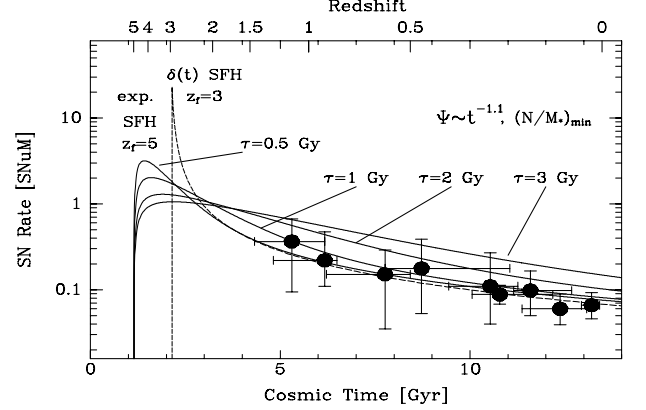


FIG. 10.— Comparison of the data to predictions of a $t^{-1.1}$ power-law DTD, convolved with an exponential SFH starting at $z_f = 5$, and several characteristic exponential times τ_{sf} . The prediction for the same DTD, but following an instantaneous burst at $z_f = 3$, shown before in Fig. 4, is plotted for comparison (dotted curve). All curves are normalized to satisfy the minimal-iron constraint. Such extended SFHs degrade the agreement with observations, and $\tau_{sf} < 2.7$ Gyr is required to avoid significantly overpredicting the rates.

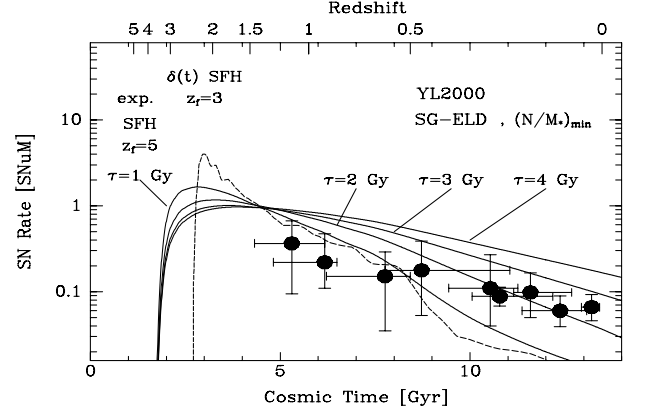


FIG. 11.— Same as Fig. 10, but for the Yungelson & Livio (2000) SG-ELD model, previously shown in Fig. 6. The convolution of this DTD with an extended exponential SFH cannot improve the fit to the SN rates, if the iron constraints on the normalization are to be simultaneously satisfied.

1 Gyr the time of initial star formation to $t_f = 1.1$ Gyr, corresponding to $z_f = 5$. Nonetheless, in every case, the fit with an extended SFH is worse than in the case of an instantaneous burst.

These results are illustrated with two examples. Figure 10 shows the predictions of a minimal-iron-normalized $t^{-1.1}$ power-law DTD, with the exponential SFH starting at $z_f = 5$, and several characteristic exponential times τ_{sf} . Also shown, for comparison, is the $z_f = 3$ instantaneous burst, shown before in Fig. 4. At late times, all the predictions have similar slopes, while at progressively shorter times, the rate dependence is shallower for the more extended SFHs. This leads to progressively greater overprediction of the observed rates. Formally, $\tau_{sf} > 2.7$ Gyr is ruled out, based on $\chi_r^2 > 2$. Conversely, if we ignore the iron constraints and find the best-fit normalization, then the integrated number of SNe Ia is significantly lower than required by the min-

imal constraint (e.g., by a factor 2, for $\tau_{sf} = 3$ Gyr). In Fig. 11, we show the same exercise for the SG-ELD model of Yungelson & Livio (2000). It might have been hoped that the convolution with an extended SFH could moderate the steep fall at late delays of this DTD, and thus provide a better fit to the observed weak time dependence of the rates. Although the steep fall, predicted in the instantaneous burst case, is indeed moderated, the smoothing at short delays lowers the contribution from early times to the integrated SN numbers, forcing a higher overall normalization and a poor fit.

To summarize this section, the moderate slope of the observed SN rate redshift dependence at $0 < z < 1.4$, combined with the large time-integrated number of SNe Ia indicated by the iron abundance, together call for a DTD that is sharply peaked at short delays, but with a low tail out to long delays. Convolution of any of the few single-DTD models that satisfy these constraints with any simple SFH that is extended on timescales $\gtrsim 1$ Gyr only degrades the fits.

7. COMPARISON TO DTD PREDICTIONS – TWO-COMPONENT MODELS

We now examine to what degree the challenges of reproducing the observations can be overcome by the addition of free parameters that is implicit in the combination of multiple components – either two DTDs (as could be expected from the co-existence of two distinct physical SN Ia channels, e.g., DD and SD), or two components of cluster SFH, as opposed to the single bursts assumed so far.

7.1. Double DTD models

The idea of two co-existing SN Ia channels, prompt and delayed, emerged several years ago from the observation of, on the one hand, a proportionality between star-formation rate (SFR) and SN Ia rate per unit stellar mass in star forming galaxies, and on the other hand, a non-zero SN Ia rate in early-type galaxies with no current star formation (Mannucci et al. 2005, 2006; Scannapieco & Bildsten 2005; Sullivan et al. 2006). As noted in §1, this observation does not necessarily imply the existence of two separate physical channels. Instead, it could be the manifestation of a DTD from a single channel but with delays spread over a wide range of timescales. Indeed, our analysis, above, shows that single parametrized DTDs of power-law form, with indices somewhat steeper than -1 can match the observational constraints (as can some DD models that produce DTDs of this type, if they are suitably scaled up). However, some of the other theoretical DTDs, that individually are incompatible with the data because they predict no delayed SNe, can be “saved” by incorporating them into a two-channel picture.

For example, two of the models of Yungelson & Livio (2000), He-ELD and the SG-Ch, predict no SNe at long time delays. Figure 12 shows the predicted cluster rates from the combination of the He-ELD model and the DD model, discussed in § 5.2. The raw sum of these two models, as before, produces a too-small fraction (less than half) of the total number of SNe Ia indicated by the minimal iron constraint, and underpredicts all the SN rates below $z < 0.5$ (by a factor of 5). However, as seen in Fig. 12, scaling up this composite DTD by factors

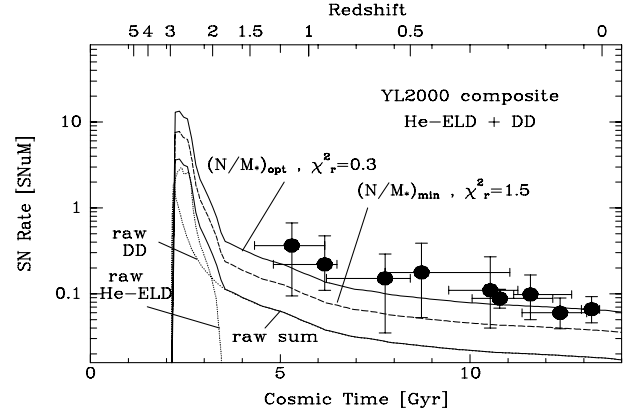


FIG. 12.— Predicted SN rate dependence for a composite DTD model, combining the He-ELD and DD models of Yungelson & Livio (2000). Dotted curves show the raw predictions of these models, and lower solid line is their sum. The raw sum underpredicts the low-redshift rates by a factor of 5 (as was the case for this DD model alone, Fig. 5), and the integrated SN number by 2.1 (minimal iron) to 3.6 (optimal iron). Scaled-up versions of these models do give a satisfactory fit to all the observations, as indicated.

of 2.1 or 3.6 can solve these problems for the minimal and optimal iron cases, respectively. In this example, 60% of the SNe (and the iron) are from the prompt He-ELD SD component, and the rest from the DD component.

Similar combinations of two components can work using the other DTDs we have considered, as long as one of the components is a DD model (or a similar power law) that can provide the SNe with long delays. In addition to the choice of components, one can choose the relative scaling between them, providing a further adjustable parameter. The current data of course cannot discriminate between the various possible prompt components as they make their contributions beyond the redshifts at which rate measurements exist. Our experiments at combining different DTD are obviously not exhaustive, but the emerging picture is nonetheless clear. The observed SN rates and the iron mass in clusters can be explained simultaneously by combining “prompt” and “delayed” DTDs. The SNe Ia from the prompt component produce the majority of the iron mass in clusters. The SNe from the delayed component produce only a fraction of the metals, and they are the events detected by current SN rate measurements, with their weak time dependence.

7.2. Composite star formation histories

A final scenario we examine is that of a single DTD, but with a composite cluster SFH, consisting of a short star-burst, beginning at z_f , combined with a more extended SFR. With the additional free parameters introduced in this scheme, it is easy to find combinations of DTDs with such composite SFHs that reproduce the SN Ia rate versus time, while simultaneously providing a sufficient time-integrated number of SNe to produce the observed ratio of iron mass to stellar mass. Figure 13 shows an example. Here, we have used the $\alpha = 1, \beta = 1$ SD model, discussed previously in §5.2, from the BPS calculations of Mennekens et al. (2010). We recall that this DTD produces only SNe Ia with short delays. In the context of the present exercise, this is desirable, as the observed SN rate dependence is generated by the SFH rather than by

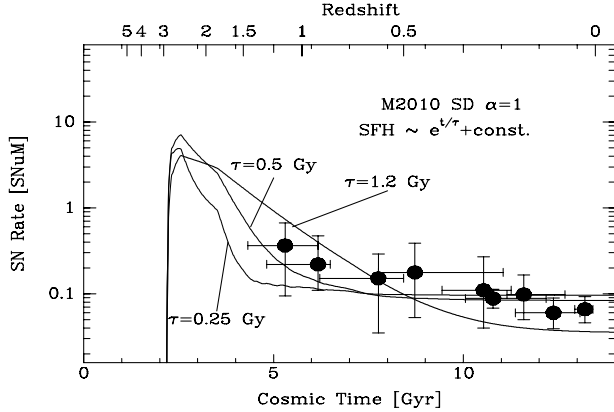


FIG. 13.— Same as Fig. 12, but with a single, prompt, DTD, and a composite SFH – an exponentially decaying burst at $z_f = 3$, with characteristic times as labeled, and a constant “DC” component of star formation, with a ratio between the components of 200:1 at $z = 3$. The DTD is the $\alpha = 1$ SD model of Mennekens et al. (2010), previously shown in Fig. 7. Normalizations are minimal-iron for the short-timescale burst and optimal-iron for the two longer-timescale bursts. As seen in the figure, such composite SFHs can match the rate observations and the iron constraints with a single, prompt, DTD. However, the constant and high level of star formation down to low redshifts is at odds with other observations of cluster galaxies.

the DTD. In this example, for the two SFH components we take the sum, $S(t) = S_1(t) + S_2(t)$, of an exponential SFR, $S_1(t) \propto \exp[-(t - t_f)/\tau_{\text{SF}}]$ as in §6, and a constant SFR, $S_2(t) = \text{const.}$ The relative levels of the two components are adjusted to fit the iron-based normalization constraints. For this choice of functions, $\tau_{\text{SF}} < 4$ Gyr is required. A more prolonged exponential component either overpredicts the high- z rates, or forces the constant component to overpredict the low- z rates.

This scenario can, in principle, explain the presently discussed data in terms of “prompt” DTDs such as those from SD models, combined with residual star formation. However, it is at odds with many other observations of clusters. Star-formation activity in clusters avoids the cluster cores ($\lesssim 1$ Mpc), and increases progressively with radius (e.g., Hansen et al 2008; Porter et al. 2008; Bai et al. 2009; Saintonge et al. 2008; Loh et al. 2008). In contrast, all of the cluster-SN candidate hosts in Sharon et al. (2010) are found at projected distances < 0.7 Mpc from the brightest cluster galaxy. In the sample of Barbary et al. (2010) all are within < 0.8 Mpc, or even < 0.5 Mpc if excluding the outermost one⁶. Furthermore, the SNe from the various surveys we analyze are almost always found in early-type, red-sequence (and hence apparently quiescent), galaxies. For example, in the sample of Gal-Yam et al. (2008), for 4 out of the 5 cluster SNe Ia that have host galaxies, the galaxies are early-types, based on colors and spectra. In the sample of Sharon et al. (2010), 6 out of the 7 most likely cluster SN Ia hosts are red-sequence galaxies. In Barbary et al. (2010), this figure is 8 out of 9. Thus, the cluster SNe Ia, on which are based the rates that we analyze, are neither at the locations nor in the types of galaxies where star-formation in clusters is actually observed to occur.

⁶ It would be useful to study the dependence of cluster SN rates on radial distance from cluster cores. Such an analysis may be feasible, however, only with a larger sample of cluster SNe.

Quantitatively, in the above version of the burst+constant SFH scenario, as shown in Fig. 13, for, e.g., $\tau_{\text{SF}} = 0.5$, $\sim 93\%$ of the present-day cluster stellar mass is formed before $z = 1$, and the remaining 7% is from the constant SFR between $z = 1$ and 0. A typical monitored stellar mass in the clusters we consider is $\sim 10^{13} M_\odot$ (see § 3.2) or, correcting to formed mass before stellar evolution mass losses, $\sim 2 \times 10^{13} M_\odot$. With a lookback time to $z = 1$ of 8 Gyr, the 7% fraction implies a constant SFR between $z = 0$ and 1 of $\sim 175 M_\odot \text{ yr}^{-1}$, just in the central regions of clusters.

By comparison, several recent studies (e.g., Krick et al. 2009, Bai et al. 2009; Koyama et al. 2010) find SFRs, integrated over the galaxies within a cluster, between ~ 10 and a few hundred $M_\odot \text{ yr}^{-1}$. Some clusters thus do have the high integrated SFRs required in the scenario of a composite SFH + prompt DTD (ignoring for the moment that this SFR is not in the central, quiescent galaxies that are seen to host the SNe, but rather in the outer regions, e.g., Haines et al. 2009). However, the observed cluster SFR, normalized by cluster mass, rises steeply with redshift, as $(1 + z)^p$, with $p = 5.3 \pm 1.2$ (Bai et al. 2009), $p = 5.7^{+2.1}_{-1.8}$ (Haines et al. 2009), or $p \approx 6$ (Koyama et al. 2010). This corresponds to one or two orders of magnitude increase in SFR over the $0 < z < 1$ range, and is in contrast to the roughly constant mass-normalized SFR that is required in this range, in the composite SFH scenario, to reproduce the cluster SN rates.

We also note that, if the DTD were universal in environment and in time, and the SFH + DTD scenario were true, then it would apply to early-type galaxies in general. SNe Ia in all early types, whether in the field or in clusters, and at low or high redshifts, would be the prompt outcome of low levels of recent but unseen star-formation in these galaxies. However, a study by Foerster & Schawinski (2008) of the early-type hosts of SNe Ia argues against this possibility. Furthermore, the DTD reconstruction in nearby galaxies by Maoz et al. (2010) demonstrates a 4σ detection of a delayed SN Ia component, with delays of $2.4 < \tau < 13$ Gyr.

We therefore conclude that the scenario of a burst+constant SFH, combined with a prompt single-component DTD, is probably not a viable model. While it is capable of explaining the cluster SN rate data and the observed iron to stellar mass ratio, it is incompatible with other cluster observations. Those observations indicate that, although about 10% of the stellar mass of clusters formed at $z < 1$, this activity did not occur in the central, quiescent, galaxies hosting the SNe found by current surveys, and that the SFR falls steeply with cosmic time, in contrast to the flat SFH required to reproduce, under this scenario, the flat observed SN rate.

8. CONCLUSIONS

Measurements of galaxy-cluster SN Ia rates as a function of cosmic time provide a particularly direct avenue to obtain the DTD of SNe Ia, with its implications for progenitor models and cosmic history. Such measurements can constrain both the functional form and the normalization of the DTD. We have combined recently completed measurements of cluster rates between $z = 0$ and $z = 1.45$ with the latest results on the iron mass content of clusters, to recover the SN Ia DTD, and to

test a variety of model DTDs, from purely mathematical parametrized forms, to DTDs obtained from more detailed physical considerations.

Our main results are as follows.

1. Assuming that the bulk of the stars in clusters formed with a normal IMF in a brief burst at $z_f \approx 3$, as indicated by optical spectroscopy of cluster galaxies, the SN Ia DTD can be directly recovered from the observations. The resulting DTD peaks at the shortest delays probed, $0 < t < 2.2$ Gyr, decreases steeply at longer delays, and extends out to 11 Gyr. The recovered DTD agrees remarkably well, both in shape and in absolute normalization, with DTDs recently recovered using different techniques, in different environments: in field ellipticals (Totani et al. 2008); in nearby galaxies (Maoz et al. 2010); and in the Magellanic Clouds (Maoz & Badenes 2010). The current derivation is complementary to previous ones in that it recovers the DTD over its full time range, with good time resolution at delays $\gtrsim 3$ Gyr. The emerging picture is of a universal DTD that is not strongly dependent on environment or cosmic time, and can be well represented by a single power law, of index $s \sim -1$.

2. Comparing the data to theoretical or phenomenological DTDs in a forward-modeling process, the best parametric description of the DTD is a power law,

$$\Psi(t) \approx 0.01 \text{ SN yr}^{-1} (10^{10} \text{ M}_{\odot})^{-1} \left(\frac{t}{1 \text{ Gyr}} \right)^s \quad (13)$$

with index $s = -1.1 \pm 0.2$ or $s = -1.3 \pm 0.2$, depending on whether we adopt a minimal-iron constraint or an optimal-iron constraint, respectively, based on cluster data. Single-component DTDs consisting of shallower power laws, such $\Psi \propto t^{-1/2}$, cannot simultaneously match the observed SN rates and the integrated SN Ia numbers dictated by the iron-to-stellar mass ratio.

3. Physical DD models from the BPS simulations we have examined can match the observations, provided they are scaled up in numbers by factors of 5 – 8. On the other hand, SD models, on their own, fail because they do not produce SNe at late delays, as implied by the data. Our results thus provide strong support for the double-degenerate SN Ia progenitor scenario.

4. The above conclusions are insensitive to the exact epoch of star formation in clusters, in the range

$z_f = 2 - 5$. The conclusions also do not change if one replaces the instantaneous starburst with an exponentially decaying SFH, except that the model fits deteriorate with increasing star-formation timescale, and so the range of acceptable models shrinks.

5. Multi-component models, that either combine freely scaled versions of two DTDs (e.g. SD and DD), or two SFH models (such as a burst plus a constant) with a prompt DTD, have enough freedom to permit many combinations that can match the existing data. However, apart from the loss of simplicity involved, such combinations face other problems. For the composite DTD models, it remains to be seen if the required combinations and scalings are physically plausible. For the composite SFHs, a high SFR in the central regions of clusters, and which remains constant between $0 < z < 1$, is required, in conflict with observations of clusters at these redshifts.

6. All of the successful DTD models produce just a fraction of the time-integrated numbers of SNe Ia at redshifts below 1.4. A clear prediction of these models is, therefore, that SN surveys of clusters or proto-clusters at even higher redshifts, approaching the stellar formation redshifts of the clusters, should reveal a sharply rising rate of SNe Ia. Alternatively, observation of a non-rising SN Ia rate would raise the possibility that the bulk of metals in clusters was produced by CC SNe from a top-heavy IMF that exploded even earlier in cluster environments.

We thank K. Barbary, M. Graham, F. Mannucci, N. Mennekens, E. Ofek, D. Poznanski, C. Pritchett, L. Yungelson, D. Zaritsky, and the anonymous referee for providing useful input. D.M. acknowledges support by a grant from the Israel Science Foundation. A.G. acknowledges support by the grant 07AST-F9 from the Ministry of Science, Culture and Sport, Israel, and the Ministry of Research, France. A.G. is also supported by the Israel Science Foundation, the EU FP7 Marie Curie program via an IRG fellowship, the Benoziyo Center for Astrophysics, Weizmann-UK, and the Peter and Patricia Gruber Awards. K.S. thanks the Benoziyo Center for Astrophysics for its hospitality in the course of this work. This work was supported by grants GO-10493 and GO-10793 from the Space Telescope Science Institute, which is operated by the Association of Universities for Research in Astronomy, Inc., under NASA contract NAS 5-26555.

REFERENCES

- Anders, E., & Grevesse, N. 1989, *Geochim. Cosmochim. Acta*, 53, 197
- Anderson, M. E., Bregman, J. N., Butler, S. C., & Mullis, C. R. 2009, *ApJ*, 698, 317
- Andreon, S., Puddu, E., de Propris, R., & Cuillandre, J.-C. 2008, *MNRAS*, 385, 979
- Andreon, S. 2010, *arXiv:1004.2785*
- Aubourg, É., Tojeiro, R., Jimenez, R., Heavens, A., Strauss, M
- Badenes, C., Maoz, D., & Draine, B. 2010, *arXiv:1003.3030*, *MNRAS*, in press
- Bai, L., Rieke, G. H., Rieke, M. J., Christlein, D., & Zabludoff, A. I. 2009, *ApJ*, 693, 1840
- Balestra, I., Tozzi, P., Ettori, S., Rosati, P., Borgani, S., Mainieri, V., Norman, C., & Viola, M. 2007, *A&A*, 462, 429
- Barbary, K., et al. 2010, *ApJ*, submitted
- Barris, B. J., & Tonry, J. L. 2006, *ApJ*, 637, 427
- Belczynski, K., Kalogera, V., Rasio, F. A., Taam, R. E., Zezas, A., Bulik, T., Maccarone, T. J., & Ivanova, N. 2008, *ApJS*, 174, 223
- Bell, E. F., McIntosh, D. H., Katz, N., & Weinberg, M. D. 2003, *ApJS*, 149, 289
- Boehringer, H., Mullis, C., Rosati, P., Lamer, G., Fassbender, R., Schwobe, A., & Schuecker, P. 2005, *The Messenger*, 120, 33
- Bogomazov, A.I. & Tutukov, A.V., 2009, *Astronomy Reports*, 53, 214
- Brandt, T. D., Tojeiro, R., Aubourg, E., Heavens, A., Jimenez, R., & Strauss, M. A. 2010, *arXiv:1002.0848*
- Bremer, M. N., et al. 2006, *MNRAS*, 371, 1427
- Bruzual, G., & Charlot, S. 2003, *MNRAS*, 344, 1000
- Buzzoni, A. 2005, *MNRAS*, 361, 725
- Cain, B., et al. 2008, *ApJ*, 679, 293
- Cappellari, M., et al. 2006, *MNRAS*, 366, 1126
- Ciotti, L., D’Ercole, A., Pellegrini, S., & Renzini, A. 1991, *ApJ*, 376, 380
- Cooper, M. C., Newman, J. A., & Yan, R. 2009, *ApJ*, 704, 687
- Daddi, E., Cimatti, A., & Renzini, A. 2000, *A&A*, 362, L45
- Dahlen, T., et al. 2004, *ApJ*, 613, 189
- Dahlen, T., Strolger, L.-G., & Riess, A. G. 2008, *ApJ*, 681, 462
- Dawson, K. S., et al. 2009, *AJ*, 138, 1271

- De Grandi, S., & Molendi, S. 2001, *ApJ*, 551, 153
- Dilday, B., et al. 2010, *ApJ*, 715, 1021
- Ebeling, H., Barrett, E., Donovan, D., Ma, C.-J., Edge, A. C., & van Speybroeck, L. 2007, *ApJ*, 661, L33
- Ehlert, S., & Ulmer, M. P. 2009, *A&A*, 503, 35
- Eisenhardt, P. R. M., et al. 2008, *ApJ*, 684, 905
- Filippenko, A. V. 1997, *ARA&A*, 35, 309
- Filippenko, A. V., et al. 2010, in preparation
- Förster, F., Wolf, C., Podsiadlowski, P., & Han, Z. 2006, *MNRAS*, 368, 1893
- Förster, F., & Schawinski, K. 2008, *MNRAS*, 388, L74
- Gal-Yam, A., Maoz, D., & Sharon, K. 2002, *MNRAS*, 332, 37
- Gal-Yam, A., & Maoz, D. 2004, *MNRAS*, 347, 942
- Gal-Yam, A., Maoz, D., Guhathakurta, P., & Filippenko, A. V. 2008, *ApJ*, 680, 550
- Gal-Yam, A., & Leonard D. C. 2009, *Nature*, 458, 865
- Gilbank, D. G., Yee, H. K. C., Ellingson, E., Hicks, A. K., Gladders, M. D., Barrientos, L. F., & Keeney, B. 2008, *ApJ*, 677, L89
- Giodini, S., et al. 2009, *ApJ*, 703, 982
- Girardi, L., Bressan, A., Bertelli, G., & Chiosi, C. 2000, *A&AS*, 141, 371
- Gonzalez, A. H., Zaritsky, D., & Zabludoff, A. I. 2007, *ApJ*, 666, 147
- Gould, A., Bahcall, J. N., & Flynn, C. 1997, *ApJ*, 482, 913
- Graham, M. L., et al. 2008, *AJ*, 135, 1343
- Greggio, L. 2005, *A&A*, 441, 1055
- Greggio, L., Renzini, A., & Daddi, E. 2008, *MNRAS*, 388, 829
- Greggio, L. 2010, *MNRAS*, 406, 22
- Grevesse, N., & Sauval, A. J. 1999, *A&A*, 347, 348
- Haines, C. P., et al. 2009, *ApJ*, 704, 126
- Han, Z., & Podsiadlowski, P. 2004, *MNRAS*, 350, 1301
- Hansen, S. M., Sheldon, E. S., Wechsler, R. H., & Koester, B. P. 2009, *ApJ*, 699, 1333
- Helder, E. A., et al. 2009, *Sceince*, 325, 719
- Hicks, A. K., et al. 2008, *ApJ*, 680, 1022
- Hoyle, F., & Fowler, W. A. 1960, *ApJ*, 132, 565
- Iben, I., Jr., & Tutukov, A. V. 1984, *ApJS*, 54, 335
- Jorgensen, H. E., Lipunov, V. M., Panchenko, I. E., Postnov, K. A., & Prokhorov, M. E. 1997, *ApJ*, 486, 110
- Kauffmann, G., et al. 2003, *MNRAS*, 341, 33
- Koyama, Y., Kodama, T., Shimasaku, K., Hayashi, M., Okamura, S., Tanaka, I., & Tokoku, C. 2010, *MNRAS*, 403, 1611
- Krick, J. E., Surace, J. A., Thompson, D., Ashby, M. L. N., Hora, J. L., Gorjian, V., & Yan, L. 2009, *ApJ*, 700, 123
- Kroupa, P., Tout, C. A., & Gilmore, G. 1993, *MNRAS*, 262, 545
- Kroupa, P. 2001, *MNRAS*, 322, 231
- Kuznetsova, N., et al. 2008, *ApJ*, 673, 981
- Laganá, T. F., Lima Neto, G. B., Andrade-Santos, F., & Cypriano, E. S. 2008, *A&A*, 485, 633
- Leaman, J., Li, W., Chornock, R., Filippenko, A. 2010, *ApJ*, submitted, arXiv:1006.4611
- Li, W., et al. 2010a, *ApJ*, submitted, arXiv:1006.4612
- Li, W., Chornock, R., Leaman, J., Filippenko, A. V., Poznanski, D., Xiaofeng, W., Ganeshalingam, M., Mannucci, F. 2010b, *ApJ*, submitted, arXiv:1006.4613
- Lin, Y.-T., Mohr, J. J., & Stanford, S. A. 2003, *ApJ*, 591, 749
- Loh, Y.-S., Ellingson, E., Yee, H. K. C., Gilbank, D. G., Gladders, M. D., & Barrientos, L. F. 2008, *ApJ*, 680, 214
- Madau, P., Della Valle, M., & Panagia, N. 1998, *MNRAS*, 297, L17
- Mannucci, F., Della Valle, M., Panagia, N., Cappellaro, E., Cresci, G., Maiolino, R., Petrosian, A., & Turatto, M. 2005, *A&A*, 433, 807
- Mannucci, F., Della Valle, M., & Panagia, N. 2006, *MNRAS*, 370, 773
- Mannucci, F., Maoz, D., Sharon, K., Botticella, M. T., Della Valle, M., Gal-Yam, A., & Panagia, N. 2008, *MNRAS*, 383, 1121
- Maoz, D. 2008, *MNRAS*, 384, 267
- Maoz, D., Mannucci, F., Li, W., Filippenko, A. V., Della Valle, M., & Panagia, N. 2010, arXiv:1002.3056, *MNRAS*, in press
- Maoz, D., & Badenes, C. 2010, arXiv:1003.3031, *MNRAS*, in press
- Maoz, D., & Gal-Yam, A. 2004, *MNRAS*, 347, 951
- Maughan, B. J., Jones, C., Forman, W., & Van Speybroeck, L. 2008, *ApJS*, 174, 117
- Mazzali, P. A., Röpke, F. K., Benetti, S., & Hillebrandt, W. 2007, *Science*, 315, 825
- Mennekens, N., Vanbeveren, D., De Greve, J. P., & De Donder, E. 2010, arXiv:1003.2491, *A&A*, in press
- Nelemans, G., & Tout, C. A. 2005, *MNRAS*, 356, 753
- Porter, S. C., Raychaudhury, S., Pimblett, K. A., & Drinkwater, M. J. 2008, *MNRAS*, 388, 1152
- Poznanski, D., et al. 2007, *MNRAS*, 382, 1169
- Pratt, G. W., Croston, J. H., Arnaud, M., Boehringer, H. 2009, *A&A*, 498, 361
- Pritchett, C. J., Howell, D. A., & Sullivan, M. 2008, *ApJ*, 683, L25
- Raskin, C., Scannapieco, E., Rhoads, J., & Della Valle, M. 2009, *ApJ*, 707, 74
- Reiss 2000, PhD thesis, University of Washington
- Renzini, A. 1997, *ApJ*, 488, 35
- Renzini, A., Ciotti, L., D'Ercole, A., & Pellegrini, S. 1993, *ApJ*, 419, 52
- Rosati, P., Stanford, S. A., Eisenhardt, P. R., Elston, R., Spinrad, H., Stern, D., & Dey, A. 1999, *AJ*, 118, 76
- Rosati, P., et al. 2004, *AJ*, 127, 230
- Ruiter, A. J., Belczynski, K., & Fryer, C. 2009, *ApJ*, 699, 2026
- Saintonge, A., Tran, K.-V. H., & Holden, B. P. 2008, *ApJ*, 685, L113
- Sadat, R., Blanchard, A., Guiderdoni, B., & Silk, J. 1998, *A&A*, 331, L69
- Salpeter, E. E. 1955, *ApJ*, 121, 161
- Scannapieco, E., & Bildsten, L. 2005, *ApJ*, 629, L85
- Sharon, K., Gal-Yam, A., Maoz, D., Filippenko, A. V., & Guhathakurta, P. 2007, *ApJ*, 660, 1165
- Sharon, K., et al. 2010, *ApJ*, 718, 876
- Sim, S. A., et al. 2010, *ApJ*, 714, L52
- Stanford, S. A., Holden, B., Rosati, P., Eisenhardt, P. R., Stern, D., Squires, G., & Spinrad, H. 2002, *AJ*, 123, 619
- Stanford, S. A., et al. 2005, *ApJ*, 634, L129
- Stanford, S. A., et al. 2006, *ApJ*, 646, L13
- Strolger, L.-G., et al. 2004, *ApJ*, 613, 200
- Sullivan, M., et al. 2006, *ApJ*, 648, 868
- Tojeiro, R., Wilkins, S., Heavens, A. F., Panter, B., & Jimenez, R. 2009, *ApJS*, 185, 1
- Totani, T., Morokuma, T., Oda, T., Doi, M., & Yasuda, N. 2008, *PASJ*, 60, 1327
- van Kerkwijk, M.H., Chang, P., Justham, S. 2010, *ApJL*, submitted, arXiv:1006.4391
- Wang, B., Li, X.-D., & Han, Z.-W. 2010, *MNRAS*, 401, 2729
- Webbink, R. F. 1984, *ApJ*, 277, 355
- Whelan, J., & Iben, I. J. 1973, *ApJ*, 186, 1007
- Woosley, S. E. 2007, *Nature Physics*, 3, 832
- Yasuda, N., & Fukugita, M. 2010, *AJ*, 139, 39
- York, D. G., et al. 2000, *AJ*, 120, 1579
- Yungelson, L. R., & Livio, M. 2000, *ApJ*, 528, 108